Available online at www.sciencedirect.com

ScienceDirect

Coastal Engineering 54 (2007) 151 – 170

Coastal Engineering
An International Journal for Coastal, Harbour and Offshore Engineers

www.elsevier.com/locate/coastaleng

Nonlinear saturation-based whitecapping dissipation in SWAN for deep and shallow water

André J. van der Westhuysen *, Marcel Zijlema, Jurjen A. Battjes

Environmental Fluid Mechanics Section, Faculty of Civil Engineering and Geosciences, Delft University of Technology, P.O. Box 5048, 2600 GA Delft, The Netherlands

Received 17 October 2005; received in revised form 8 August 2006; accepted 29 August 2006
Available online 20 October 2006

Abstract

This study investigates the effectiveness of a revised whitecapping source term in the spectral wind wave model SWAN (Simulating WAves Nearshore) that is local in frequency space, nonlinear with respect to the variance density and weakly dependent on the wave age. It is investigated whether this alternative whitecapping expression is able to correct the tendency towards underprediction of period measures that has been identified in the default SWAN model. This whitecapping expression is combined with an alternative wind input source term that is more accurate for young waves than the default expression. The shallow water source terms of bottom friction, depth-induced breaking and triad interaction are left unaltered. It is demonstrated that this alternative source term combination yields improved agreement with fetch- and depth-limited growth curves. Moreover, it is shown, by means of a field case over a shelf sea, that the investigated model corrects the erroneous overprediction of wind-sea energy displayed by the default model under combined swell-sea conditions. For a selection of field cases recorded at two shallow lakes, the investigated model generally improves the agreement with observed spectra and integral parameters. The improvement is most notable in the prediction of period measures.

Keywords: SWAN; Whitecapping dissipation; Wind–wave spectra; Wave period; Combined wind-sea and swell

1. Introduction

The spectral wind wave model SWAN (Booij et al., 1999) is a widely used tool for the computation of wave fields over shelf seas, in coastal areas and shallow lakes. The accurate estimation of wave statistics by such models is important to various engineering applications in these environments. SWAN computes the evolution of wave action density N using the action balance equation (Booij et al., 1999):

$$\frac{\partial N}{\partial t} + \nabla_{x,y} \cdot [(\vec{c}_g + \vec{U})N] + \frac{\partial}{\partial \theta}(c_\theta N) + \frac{\partial}{\partial \sigma}(c_\sigma N) = \frac{S_{\mathrm{tot}}}{\sigma} \quad (1)$$

with

$$S_{\mathrm{tot}} = S_{\mathrm{in}} + S_{\mathrm{wc}} + S_{\mathrm{nl4}} + S_{\mathrm{bot}} + S_{\mathrm{brk}} + S_{\mathrm{nl3}}. \quad (2)$$

The terms on the left-hand side represent, respectively, the change of wave action in time, the propagation of wave action in geographical space (with $\vec{c}_g$ the wave group velocity vector and $\vec{U}$ the ambient current), depth- and current-induced refraction (with propagation velocity c_θ in directional space θ) and the shifting of the radian frequency σ due to variations in mean current and depth (with the propagation velocity c_σ). The right-hand side represents processes that generate, dissipate or redistribute wave energy. In deep water, three source terms are used: the transfer of energy from the wind to the waves, S_{in}; the dissipation of wave energy due to whitecapping, S_{wc}; and the nonlinear transfer of wave energy due to quadruplet (four-wave) interaction, S_{nl4}. In shallow water, dissipation due to bottom friction, S_{bot}, depth-induced breaking, S_{brk}, and nonlinear triad (three-wave) interaction, S_{nl3}, are additionally accounted for.

The application of SWAN to a range of field situations has shown that significant wave height tends to be well predicted, but that period measures are typically somewhat underestimated (e.g. Bottema et al., 2003; Rogers et al., 2003). The

* Corresponding author. Tel.: +31 15 278 3255; fax: +31 15 278 4842.
E-mail address: A.J.vanderWesthuysen@tudelft.nl
(A.J. van der Westhuysen).

0378-3839/$ - see front matter © 2006 Elsevier B.V. All rights reserved.
doi:10.1016/j.coastaleng.2006.08.006

underprediction of period measures is related to the following: for pure wind-sea, the energy density at lower frequencies is typically underpredicted, whereas energy levels in the tail are generally overpredicted. These leave both the peak and mean periods underpredicted. In combined swell-sea situations, SWAN predicts higher dissipation of swell in the presence of wind-sea than without it, whereas the wind-sea part of the spectrum experiences reduced dissipation in the model due to the presence of the swell, leading to accelerated wave growth (Hurdle, 1998; Holthuijsen and Booij, 2000). This behaviour is at odds with the observations in the field and the laboratory, for example Donelan (1987), which suggests that the presence of low-frequency waves may actually reduce the growth of the wind-sea part of the spectrum, while the swell energy is not dissipated.

The unsatisfactory model performance described above is found both in deep and shallow water situations and could therefore be the combined result of deficiencies in both deep and shallow water source terms. However, we will focus our attention here on the deep water terms. In default mode, SWAN uses the wind input and whitecapping expressions of Komen et al. (1984), with wind input based on Snyder et al. (1981) and whitecapping based on Hasselmann (1974), together with the Discrete Interaction Approximation (DIA) for quadruplet interaction (Hasselmann and Hasselmann, 1985). Of these three, the wind input based on Snyder et al. (1981) is the best-established experimentally, at least for light winds over fairly mature wind-sea. Quadruplet interaction, although difficult to measure experimentally, is well-established theoretically for homogeneous, random-phase wave fields. Van der Westhuysen et al. (2005) demonstrate that the peak period underprediction by SWAN is partly due to the use of the DIA, which is an approximation of the complete set of quadruplet interactions described by Hasselmann (1962). In comparison, there is much uncertainty concerning the physical mechanism of whitecapping in deep and shallow water and hence the appropriate form for its source term. The expressions available for whitecapping are therefore mostly speculative. The model errors described above can readily be related to the whitecapping formulation of Komen et al. (1984): it has been found that the erroneous model behaviour in the presence of swell is caused by the expression's dependence on the mean spectral wavenumber and steepness (Hurdle, 1998), and that the overprediction of energy levels in the tail appears to be caused by insufficient dissipation in this spectral region (Rogers et al., 2003).

A number of modifications to the whitecapping expression have been proposed in the literature to improve the simulation results of SWAN. A first group of modifications considers pure wind-sea conditions: Booij et al. (1999) apply a rescaled version of the Komen et al. (1984) whitecapping formulation in combination with the wind input expression of Janssen (1991) (the so-called WAM Cycle 4 physics, see Komen et al., 1994). They find, however, that this source term combination produces less accurate predictions of significant wave height and peak period than the default model. Rogers et al. (2003) alter the weighting of the relative wavenumber factor in the Komen et al. (1984) whitecapping formulation, by which the distribution of dissipation over frequency is changed. This compensates for the peak period underprediction caused by the DIA, in addition to increasing dissipation in the tail region. Within the observation range of Kahma and Calkoen (1992) this leads to improved period measures, but unfortunately wave energy is overestimated as a result (Fig. 1).

The second group of modifications considers combined swell-sea situations: Holthuijsen and Booij (2000) suggest that the dependence of wind-sea dissipation on swell in the Komen et al. (1984) expression be removed by making the dissipation at a particular frequency a function of the mean wavenumber and steepness of only the frequencies higher than itself. This method succeeds in removing the dependence of wind-sea dissipation on swell, but does not appear to be based on any physical considerations. Furthermore, this method retains the problem of enhanced dissipation of swell in the presence of wind-sea. Hurdle and Van Vledder (2004) propose an opposite approach (the so-called Cumulative Steepness Method, CSM), where dissipation at a particular frequency depends on the cumulative steepness of all spectral components *up to* the frequency considered, rather than on the mean values of wavenumber and steepness. This approach is based on the principle of surface straining, by which shorter waves are steepened by their superposition on longer waves, thus inducing breaking. Hurdle and Van Vledder demonstrate that their dissipation source term successfully decouples the growth of wind-sea from the presence of low-energy swell, but their model variant does not reproduce fetch-limited growth curves for pure wind-sea very well (Fig. 1). Rogers et al. (2003) propose to disallow the dissipation of swell energy, so that the dissipation of swell in

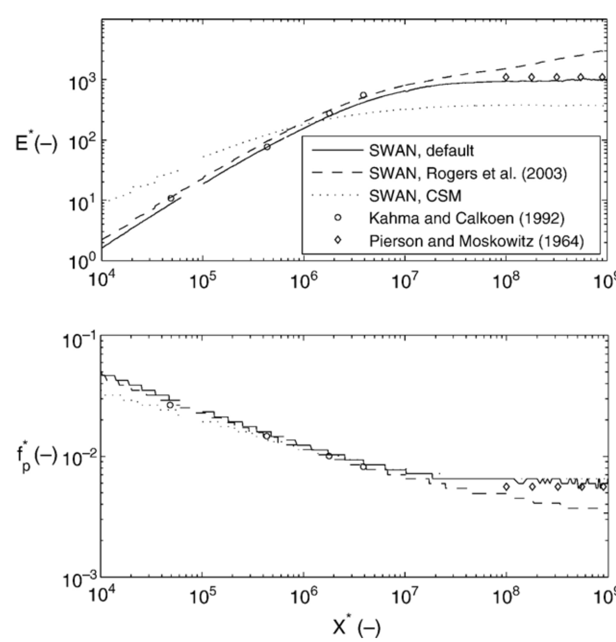

Fig. 1. Comparison of the deep water, fetch-limited growth curves produced using Komen et al. (1984) source terms (default model) with those produced using the Rogers et al. (2003) and CSM alternatives for whitecapping. In all cases the DIA is used for quadruplet interaction. Results for $U_{10}=10$ m/s, presented in terms of dimensionless energy $E^*=g^2E_{tot}/u_*^4$ and peak frequency $f_p^*=f_pu_*/g$ as functions of dimensionless fetch $X^*=gX/u_*^2$, with friction velocity u_* calculated using Wu (1982).

combined swell-sea conditions is prevented. The spurious influence of swell on wind-sea, however, is not addressed. Recently, Bidlot et al. (2005) proposed to redefine the mean spectral wavenumber used in the Komen et al. (1984) white-capping expression to $\tilde{k}_{BAJ} = [\int \sqrt{k}E(\vec{k})\mathrm{d}\vec{k}/\int E(\vec{k})\mathrm{d}\vec{k}]^2$, by which more weight is given to the higher wavenumbers (the conventional definition is given in Section 2.1). Ardhuin et al. (in press) show that this altered parameterisation of the wavenumber reduces, but does not eliminate the spurious effect of swell on wind-sea generation. This result strengthens the case against the use of spectral mean variables in whitecapping expressions.

Many alternative dissipation formulations exist besides those implemented in SWAN which were reviewed above. Donelan and Yuan (1994) distinguish between the following classes of models for dissipation due to wave breaking: whitecap models (e.g. Hasselmann, 1974 in SWAN), probability models (e.g. Longuet-Higgins, 1969a) and quasi-saturated models (e.g. Phillips, 1985). Recently, a line of investigation that relates breaking probability to local spectral steepness was initiated, prompted by the apparent link between deep water wave breaking and wave groups observed by Donelan et al. (1972) and Holthuijsen and Herbers (1986), amongst others. Assuming that dissipation occurs within wave groups, Banner et al. (2000) demonstrated that the mean steepness of dominant waves (integrated over a bandwidth around the spectral peak) is well-correlated with their breaking probability, prompting them to propose this quantity as the primary variable determining the breaking of dominant waves. It was also found that there is a dominant wave steepness below which no breaking was observed: the so-called breaking threshold. It is noted here, however, that the relation obtained between dominant wave steepness and the breaking probability of these waves does not necessarily constitute a causal link between wave groups and the primary breaking mechanism. Banner et al. (2002) extend the study of Banner et al. (2000) to investigate the breaking probability over spectral intervals up to 2.48 times the spectral peak frequency. In their study, the mean steepness parameter used by Banner et al. (2000) is replaced by the spectral saturation as a convenient, bandwidth-independent measure of the local spectral steepness. Banner et al. (2002) demonstrate a relation between the saturation spectrum and breaking probability across the spectrum from the peak frequency f_p to $2.48f_p$, and found that, also in this spectral region, breaking only commences once a saturation threshold has been reached. Alves and Banner (2003) incorporate these findings into a dissipation formulation, proposing an expression that features a primary dependence on the (frequency-local) spectral saturation.

A central question regarding expressions for dissipation due to breaking is whether the dissipation is local or broad-banded in frequency space. From experimental data, Phillips et al. (2001) and Melville and Matusov (2002) find that the dissipation is local in frequency space, whereas Banner et al. (1989) and, very recently, Young and Babanin (2006) present evidence that, in addition to dissipating energy locally, breaking longer waves dissipate energy of shorter waves too. Although breaking is considered to be the main mechanism of wave energy dissipation, additional dissipation is possible due to, for example, the interaction of waves with turbulence (e.g. Ardhuin and Jenkins, 2006) and interactions between long and short waves (Longuet-Higgins, 1969b; Hasselmann, 1971). Independent formulations for such mechanisms do exist, but they still require much development.

In this study, a new set of deep water source terms, featuring a wave breaking expression based on that of Alves and Banner (2003), is implemented in SWAN to address the inaccuracies concerning period measures reviewed above. The saturation-based expression of Alves and Banner (2003) regards dissipation as essentially local in wavenumber space, and consequently offers a way to resolve the spurious behaviour of SWAN under combined swell-sea conditions. However, a number of elements of the Alves and Banner (2003) expression, as calibrated, are revised in this study: firstly, the level of the saturation threshold used by Alves and Banner is considered too high, so that it essentially loses the meaning ascribed to it by Banner et al. (2000) and Banner et al. (2002). In the present study, the level of the saturation threshold is returned to the value range found by Banner et al. (2002). Secondly, the calibrated dissipation expressions of Alves and Banner are highly nonlinear functions of the variance density, apparently without justification. In this study, the dissipation expression is made to scale similarly to the wind input term, based on the theoretical work of Phillips (1985) and Resio et al. (2004). This approach is akin to those applied by Donelan (2001) and Hwang and Wang (2004). Thirdly, Alves and Banner introduce multiplication factors that are dependent on mean spectral steepness and wavenumber to their formulation to approximate the additional influences of interaction with turbulence and short-wave–long-wave interactions. These factors re-introduce some dependence on spectral mean quantities to the expression. Also, frequency-local breaking dissipation is hereby lumped together with other forms of dissipation that are better modelled separately and more comprehensively, as in Teixeira and Belcher (2002) (dissipation due to turbulence) and Young and Babanin (2006) (short-wave dissipation due to the breaking of dominant waves). We have therefore chosen to remove these dependencies, retaining an expression based on frequency-local breaking only. Our proposed dissipation expression is used together with a wind input term based on that of Yan (1987), which is a combination of Plant (1982)'s expression for strongly forced waves with that of Snyder et al. (1981) for weakly forced waves. Based on the scaling arguments of Phillips (1985) and Resio et al. (2004), the choice of parameters for the dissipation term is made in such a way that it has the same frequency scaling as the wind input term. This yields a whitecapping source term that has a secondary dependence on wave age. The resulting source term combination is calibrated against fetch- and depth-limited growth curves and subsequently evaluated for a shelf-sea field case with combined swell-sea wave conditions and a number of finite depth field cases, where it will be shown to yield satisfactory results.

In the greater part of this study, nonlinear quadruplet interactions are calculated using the DIA. However, some characteristic effects of using a complete representation of quadruplet interactions (using the WRT exact code, as re-programmed by Van Vledder, 2005) are also presented.

The structure of this paper is as follows: Section 2 presents the default and new saturation-based source terms investigated in this study. Section 3 presents simulations with the saturation-based and default models, including the calibration of the new model, its evaluation for various field cases and its performance in combination with exact quadruplet calculation. Section 4 closes the paper with discussion and conclusions.

2. Modelling approach

This section presents the current default source terms for wind input and whitecapping used in SWAN, and describes the new source term combination investigated in this study, which features nonlinear saturation-based whitecapping dissipation. The section closes with a description of the parameter choice for the new source term combination in deep and finite depth water.

2.1. Default source terms

2.1.1. Whitecapping dissipation

Whitecapping dissipation is currently represented in SWAN by the pulse-based, quasi-linear model of Hasselmann (1974). The formulation used in the model is based on that of Komen et al. (1984):

$$S_{\mathrm{wc}}(\sigma,\theta) = -C_{\mathrm{ds}}\left(\frac{k}{\tilde{k}}\right)^{q}\left(\frac{\tilde{s}}{\tilde{s}_{\mathrm{PM}}}\right)^{r}\tilde{\sigma}E(\sigma,\theta) \tag{3}$$

in which k is the wavenumber, with a spectral mean $\tilde{k}$, and $\tilde{\sigma}$ is the spectral mean radian frequency. These are defined as $\tilde{k}=[E_{\mathrm{tot}}/\iint k^{-1/2}E(\sigma,\theta)\mathrm{d}\sigma\mathrm{d}\theta]^2$ and $\tilde{\sigma}=E_{\mathrm{tot}}/\iint \sigma^{-1}E(\sigma,\theta)\mathrm{d}\sigma\mathrm{d}\theta$, where E_{tot} is the total spectral variance. Quantity $\tilde{s}$ is the mean spectral steepness, defined as $\tilde{k}\sqrt{E_{\mathrm{tot}}}$, and $\tilde{s}_{\mathrm{PM}}$ is the mean steepness of the Pierson–Moskowitz spectrum. The tuning parameters of this expression are C_{ds}, q and r. The default setting is $C_{\mathrm{ds}}=2.36\times10^{-5}$, $q=1$ and $r=4$. Note the strong dependence of this expression on the mean spectral steepness $\tilde{s}$ and wavenumber $\tilde{k}$.

2.1.2. Wind input

The current default expression for exponential wave growth due to wind is the formulation of Komen et al. (1984), which is based on the empirical results of Snyder et al. (1981):

$$\begin{aligned}\beta_{\mathrm{Snyder}}(\sigma,\theta) &= \frac{1}{\sigma E}S_{\mathrm{in}}(\sigma,\theta)\\ &= \max\left[0,\ 0.25\frac{\rho_{\mathrm{a}}}{\rho_{\mathrm{w}}}\left(28\frac{u_*}{c}\cos(\theta-\alpha)-1\right)\right]\end{aligned} \tag{4}$$

where ρ_{a} and ρ_{w} are the densities of air and water respectively, u_* is the friction velocity of the wind, c the wave phase velocity and α the wind direction. Expression (4) is based on field measurements of weakly forced waves ($1<U_5/c<3$) where U_5, the wind speed at 5 m height, had rather low values of 5–7 m/s. Hasselmann and Bösenberg (1991) extended this study for conditions more typical of those in the open ocean, with wind speeds in the range $U_5=2$–12 m/s. Their data, which had a comparable wind forcing range of $1<U_5=c<2.5$, yielded a wind input expression similar to (4). Therefore, (4) seems to be well-established for weakly forced conditions, but its proven validity does not extend to the strongly forced conditions of young wave fields.

2.2. Saturation-based model

2.2.1. Whitecapping dissipation

The whitecapping formulation investigated in this study is based on that of Alves and Banner (2003), which has a primary dependence on the azimuthal-integrated spectral saturation $B(k)$:

$$S_{\mathrm{wc}}(k,\theta) = -C_{\mathrm{ds}}\left[\frac{B(k)}{B_{\mathrm{r}}}\right]^{p/2}\underbrace{(E_{tot}k_p^2)^m}_{A}\underbrace{\left(\frac{k}{\tilde{k}}\right)^n}_{B}\sigma\Phi(k,\theta) \tag{5}$$

where $\Phi(k,\theta)$ is the polar wavenumber spectrum (defined such that $E_{\mathrm{tot}}=\int_0^{2\pi}\int_0^{\infty}\Phi(k,\theta)k\,\mathrm{d}k\,\mathrm{d}\theta$), B_{r} a threshold saturation level, $E_{\mathrm{tot}}k_{\mathrm{p}}^2$ an integral steepness parameter and C_{ds}, m and n tunable parameters. The azimuthal-integrated spectral saturation $B(k)$, which is closely related to spectral steepness, is given by Banner et al. (2002) as

$$B(k) = \int_0^{2\pi} k^4\Phi(k,\theta)\mathrm{d}\theta. \tag{6}$$

When $B(k)>B_{\mathrm{r}}$, waves break, and the exponent p is set equal to a constant calibration parameter p_0. For $B(k)<B_{\mathrm{r}}$ there is no breaking, and the dissipation based on $B(k)$ gives way to other sources of dissipation (see below) by setting p to zero. A smooth function is used by Alves and Banner to make the transition between these two extremes:

$$p = \frac{p_0}{2}+\frac{p_0}{2}\tanh\left\langle 10\left(\left[\frac{B(k)}{B_r}\right]^{1/2}-1\right)\right\rangle. \tag{7}$$

By means of numerical simulation and comparison against spectral and integral observations, Alves and Banner (2003) propose using values of B_{r} in the range 3.10×10^{-3} to 4.25×10^{-3} and $p_0=4$ to 8. These values of B_{r} are about double the (non-normalised) threshold saturation values found by Banner et al. (2002), so that they cannot be ascribed the meaning of a saturation threshold. Furthermore, the high values of p_0 imply a dependence of dissipation on the variance density of up to a power of 5. It is unclear how such high rates of dissipation can be balanced by conventional wind input expressions such as those of Snyder et al. (1981), Plant (1982) or Janssen (1991). In the present study these shortcomings are addressed by *a priori* limiting the value of B_{r} to the range 1.5–2.0×10^{-3} in accordance with Banner et al. (2002), and by choosing p_0 such a balance is maintained between the source terms of that wind input, dissipation and quadruplet interaction. A third perceived shortcoming of (5) is that the primary dissipation mechanism based on $B(k)$ is supplemented with two multiplication factors in order to represent dissipation due to general background turbulence (factor A) and long-wave–short-wave interactions (factor B). These were included by Alves and Banner to obtain greater tunability over a wide range of wave ages. However, as discussed in the introduction, these factors re-introduce mean spectral dependencies to the expression. Moreover, being multiplication factors rather than separate terms in a sum, they also oversimplify the influence that turbulence and longer waves may have on the wave field, so that they cannot be expected to perform well in the representation of these processes. We therefore chose to eliminate the influence of these factors by setting the exponents m and n equal to zero, reducing (5) to its dependence on frequency-local wave breaking only. Omitting A and B, and transforming (5) into frequency space (but retaining $B(k)$ and B_r in wavenumber space and replacing σ by $g^{\frac{1}{2}}k^{\frac{1}{2}}$) leads to the dissipation expression

$$S_{\mathrm{wc}}(\sigma,\theta) = -C_{\mathrm{ds}}\left[\frac{B(k)}{B_{\mathrm{r}}}\right]^{p/2} g^{\frac{1}{2}}k^{\frac{1}{2}}E(\sigma,\theta) \tag{8}$$

where $B(k)$ is calculated from frequency space variables as follows

$$B(k) = \int_0^{2\pi} \frac{\mathrm{d}\sigma}{\mathrm{d}k}k^3E(\sigma,\theta)\mathrm{d}\theta = c_{\mathrm{g}}k^3E(\sigma). \tag{9}$$

As mentioned above, the choice of the exponent p is made by taking into consideration the balance between the deep water source terms, as will be described in Section 2.3 below. This leaves C_{ds} and B_{r} as the only remaining tuning parameters of (8).

2.2.2. Wind input

Since the present study is mainly concerned with the effects of altering the whitecapping formulation in SWAN, we restrict the scope here to established empirical expressions for wind input. For strongly forced waves ($u_*/c>0.1$) a wide variety of laboratory results (e.g. Plant, 1982; Peirson and Belcher, 2005) and some field observations (e.g. Hsiao and Shemdin (1983)) point to a quadratic dependence of the wind-induced growth rate on the wind forcing parameter u_*/c. Under weaker wind forcing ($u_*/c<0.1$) a linear dependence on u_*/c, as used in (4), seems to hold (Snyder et al., 1981; Hasselmann and Bösenberg, 1991). Expressions such as that of Hsiao and Shemdin (1983) and Yan (1987) unify these two observational ranges. Yan (1987) proposes an analytical fit through the experimental datasets of Snyder et al. (1981) and Plant (1982) of the form

$$\begin{aligned}\beta_{\mathrm{fit}} = D\left(\frac{u_*}{c}\right)^2\cos(\theta-\alpha) + E\left(\frac{u_*}{c}\right)\cos(\theta-\alpha) \\ + F\cos(\theta-\alpha) + H\end{aligned} \tag{10}$$

where D, E, F and H are coefficients of the fit. Yan proposes the parameter values $D=4.0\times10^{-2}$, $E=5.44\times10^{-3}$, $F=5.5\times10^{-5}$ and $H=-3.11\times10^{-4}$, which produces a reasonable fit between the curves of Snyder et al. and Plant. However, Yan's fit yields a smaller growth rate than the Snyder et al. expression for mature waves (for u_*/c lower than 0.054). Yan (1987) confirms that this leads to an underestimation of the evolution of mature waves compared to that produced using Snyder et al.'s expression. We have therefore refitted (10) to better match Snyder et al.'s expression for mature waves. This yielded parameter values of $D=4.0\times10^{-2}$, $E=5.52\times10^{-3}$, $F=5.2\times10^{-5}$ and $H=-3.02\times10^{-4}$. It is this refitted expression that is used throughout the present study.

2.3. Parameter choice for saturation-based model

In choosing the parameter p in the dissipation term (8), which affects the expression's frequency scaling, it was aimed to arrive at a spectral shape that corresponds with the observations in the field. A robust feature of observed spectra is the f^{-4} shape of the energy-containing part of the spectral tail (Toba, 1973; Donelan et al., 1985; Battjes et al., 1987). Nonlinear quadruplet interactions have been ascribed a central role in maintaining the characteristic shape of wind–wave spectra (Young and Van Vledder, 1993). Resio and Perrie (1991) have shown that in deep water, in the absence of other source terms, quadruplet interactions will tend to maintain the spectrum in a f^{-4} shape at frequencies higher than 1.5 times the peak frequency. Phillips (1985) proposes that in the equilibrium range, at frequencies much higher than the peak, a statistical equilibrium exists between the source terms of wind input, dissipation and nonlinear interaction. Assuming that S_{in} is proportional to $(u_*/c)^2$, Phillips finds that these three terms should all scale similarly with frequency. Starting from the same assumption of statistical equilibrium, Resio et al. (2004) suggest that it is only required that the terms of wind input and dissipation scale similarly with frequency to recover a deep water f^{-4} shape from the balance. Following the latter, we require that the dissipation term (8) should have the same frequency scaling as the wind input expression (10), which is proportional to $(u_*/c)^2$ for strongly forced wave components. This is achieved by constraining the exponent p in (8) to 4 for $u_*/c>0.1$. For a tail shape of f^{-4}, the dissipation source term (8) then scales like f^{-1}, similar to the scaling of (10) for a high u_*/c (see Appendix A).

As the wave field gets older, its wind forcing u_*/c decreases over the energy-containing tail region. According to Resio and Perrie (1991) the quadruplet interactions still strive to maintain a f^{-4} shape over frequencies higher than 1.5 times the peak frequency. We therefore once again require that wind input and dissipation scale similarly with frequency to recover a spectral tail shape of f^{-4}. Under this weaker forcing, the wind input expression (10) goes over to a linear proportionality to u_*/c. To obtain similar frequency scaling, the exponent p in (8) should take the value 2 (Appendix A). It is therefore proposed that the parameter value p gradually changes from 4 to 2 as the wind input source term (10) goes over from a $(u_*/c)^2$ to a (u_*/c) proportionality. This suggests a secondary dependence of whitecapping on wave age, with decreasing dissipation intensity as wave age increases. Dependence of dissipation on wave age has been observed in the field by a number of investigators. Longuet-Higgins and Smith (1983) and Katsaros and Atakturk (1992) find that breaking probability increases proportionate to wind speed (or stress) and inverse wave age, and propose empirical expressions for breaking probability using these variables. More recently, Banner et al. (2000) and Babanin et al. (2001) find that for a diverse range of field situations the inclusion of wave age in the breaking determinant (alongside steepness as primary parameter) improves correlation in the prediction of breaking events. It can therefore be concluded that some dependence of the whitecapping source term on wave age appears to be justified.

Following the arguments above, the exponent p in (8), written as p_0 if $B(k)>B_r$, is constrained to $p_0=4$ for $u_*/c>0.1$ and $p_0=2$ for $u_*/c<0.1$. This is achieved by a simple transition expression for p_0, centred on $u_*/c=0.1$:

$$p_0(u_*/c) = 3 + \tanh\left[w\left(\frac{u_*}{c} - 0.1\right)\right]. \tag{11}$$

where w is a shape parameter by which a smooth transition is obtained. A value of $w=26$ is used here.

The scaling arguments above apply where $B(k)>B_r$ and waves break. According to Alves and Banner (2003), breaking-based dissipation, dependent on $B(k)$, should cease where $B(k)$ is smaller than the threshold B_r. However, model runs showed that over these spectral regions, typically somewhat below the peak frequency, a small amount of residual dissipation is required to ensure that an equilibrium growth level is reached at longer fetches. Following Alves and Banner, a transition between saturation-based dissipation and this residual dissipation is achieved with (7), in which the exponent p reduces to zero for $B(k)<B_r$, and has a value of p_0 otherwise. On incorporating (11) and (7) in (8), the resulting dissipation expression has a cubic dependence on variance density for young, strongly forced waves and a quadratic dependence on variance density for mature, weakly forced waves.

2.4. Shallow water effects

Relatively little is known about the influence of finite water depth on the wave spectrum and the source terms of wind input, whitecapping and quadruplet interactions. Some guiding observations are available, however, and these were used to adapt the source term balance discussed above for use in finite water depths:

(a) Concerning whitecapping, Babanin et al. (2001) show that, upon correcting for breaking events due to depth restriction, data collected in the shallow Lake George ($0.7<kd<2.0$, where d is the water depth) fit the relationship between breaking probability and frequency-local steepness established for deep water by Banner et al. (2000). This supports the applicability of the dissipation expression presented in Section 2.2 to finite depth environments.

(b) Concerning quadruplet interaction, a number of authors (e.g. Hashimoto et al., 2003; Van Vledder and Bottema, 2003) have demonstrated that, according to the formulation of Hasselmann (1962), the interactions are significantly influenced by finite water depth. Yet, Resio et al. (2001) show that in water of finite depth–up to the surf zone–the shape stabilisation characteristic of quadruplet interaction yields an equilibrium tail shape of $F(k) \propto k^{-2.5}$, where $F(k)$ is the one-dimensional wavenumber spectrum, conforming to the deep water observations by e.g. Toba (1973) and Donelan et al. (1985). As the water depth further decreases, however, quadruplet interaction gives way to triad (three-wave) interaction as the dominant nonlinearity. This transition is reflected in the limitation in the applicability of the weakly nonlinear theory for quadruplet interaction in such regions. Zakharov (1999) shows that the weakly nonlinear theory is only valid for wave components for which $(ak)^2 \ll (kd)^5$, where a is the amplitude of the wave component.

(c) Concerning wind forcing, relations obtained in deep water are conventionally applied unaltered to finite water depth environments, except for the fact that the wind forcing parameter u_*/c may increase due to depth limitation. This approach has also been followed in the present study. Very recently, however, Donelan et al. (2006) have provided field evidence that the increase in steepness of highly forced wind seas (being either very young or strongly depth-limited) may affect their growth rates significantly due to sheltering and flow separation. These effects are not included in the present study, but their potential impact is discussed in Sections 3 and 4.

(d) Concerning the wave spectrum, Kitaigorodskii et al. (1975) show that the deep water frequency spectrum gets affected by shallow water due to the shoaling and depth-induced breaking of its constituent waves. Bouws et al. (1985) propose that the frequency spectrum is transformed from $E(f) \propto f^{-5}$ in deep water to $E(f) \propto f^{-3}$ in very shallow water (the so-called TMA spectrum), based on an assumption that $F(k) \propto k^{-3}$ in deep and shallow water. By contrast, Miller and Vincent (1990) argue that the transition from deep to shallow water is rather from $E(f) \propto f^{-4}$ to $f^{-2.5}$, on the assumption of a tail shape in wavenumber space of $F(k) \propto k^{-2.5}$(the so-called FRF spectrum).

The findings of Miller and Vincent (1990) and Resio et al. (2001) are in agreement with each other and also with the spectral shape of Donelan et al. (1985) that we have assumed for deep water. These results are therefore used as a basis for scaling the dissipation expression (8) for finite water depths. Assuming that quadruplet interactions will maintain a tail shape of $F(k) \propto k^{-2.5}$ infinite depth too, the same scaling arguments applied in Section 2.3 will maintain an $F(k) \propto k^{-2.5}$ spectral tail for the combination of all three deep water source terms as the water depth decreases. Appendix A shows that for weakly forced waves, $u_*/c<0.1$ say, where $S_{in} \propto u_*/c$, the expressions (8) and (10) have similar scaling also infinite depth. However, for strongly forced waves, $u_*/c>0.1$ say, where $S_{in}(u_*/c)^2$, the scaling of the wind input expression (10) in finite depth differs from that of the whitecapping expression (8) by a dimensionless factor of $[\tanh(kd)]^{-1/2}$. Therefore, in order to obtain the desired equal scaling of these two source terms in finite depth, the whitecapping expression is adapted to

$$S_{\mathrm{wc}}(\sigma,\theta) = -C_{\mathrm{ds}}\left[\frac{B(k)}{B_{\mathrm{r}}}\right]^{p/2}[\tanh(kd)]^{\frac{2-p_0}{4}} g^{\frac{1}{2}} k^{\frac{1}{2}} E(\sigma,\theta) \quad (12)$$

which reduces to (8) in weakly forced or deep water conditions. Due to the factor $[\tanh(kd)]^{(2-p_0)/4}$, strongly forced waves will experience increased dissipation in finite depth. In practice, however, this addition was found to have relatively little effect.

As mentioned above, the dominance of the source terms of wind input, whitecapping and especially quadruplet interaction decreases with decreasing water depth. Consequently, in very shallow water (defined by a high Ursell number, a high wave height-over-depth ratio, or Zakharov's $(ak)^2 \approx (kd)^5$) the source term balance and spectral shape described above will give way to a balance determined by the shallow water source terms of bottom friction, depth-induced breaking and triad nonlinear interactions.

3. Simulations

This section investigates the performance of the saturation-based model described above in SWAN, and compares this performance to that of the default model. First, the calibration of the saturation-based model by means of fetch- and depth-limited growth curves is outlined. Subsequently, the calibrated model is evaluated for a number of field cases, including a shelf sea with a combined swell-sea wave field, and two shallow lakes. Finally, the performance of the saturation-based model in combination with an exact method for the calculation of quadruplet interactions is investigated.

3.1. Calibration

In this section, the calibration of the saturation-based model (10) and (12), when combined with the DIA quadruplet expression, is presented. First, the calibration of this model for deep water fetch-limited conditions is outlined, followed by the calibration for finite depth conditions, where wave growth is limited by depth, rather than fetch or duration. All the simulations presented in this section were performed in stationary mode, with a sufficient number of iterations to ensure convergence.

3.1.1. Fetch-limited growth

The calibration of the saturation-based model for deep water was done by means of a series of nested one-dimensional simulations, with a geographical discretisation ranging from 1 m (at short fetches) to 10 km (at long fetches) and frequency and directional resolutions of $\Delta\sigma/\sigma = 0.1$ and $\Delta\theta = 10°$ respectively. Fig. 2 presents the deep water fetch-limited growth curves produced by the saturation-based model when the parameters of (12) are calibrated to $C_{\mathrm{ds}} = 5.0\times10^{-5}$ and $B_{\mathrm{r}} = 1.75\times10^{-3}$ and where p_0 varies according to (11). By means of comparison, the fetch-limited growth curves produced by the default model are also shown. Here $E^* = g^2E_{\mathrm{tot}}/u_*^4$ and $f_{\mathrm{p}}^* = u_*f_{\mathrm{p}}/g$ are the dimensionless energy and peak frequency respectively and $X^* = gX/u_*^2$ the dimensionless fetch. In the top panels of Fig. 2 it can be seen that both model variants (a) reproduce dimensionless

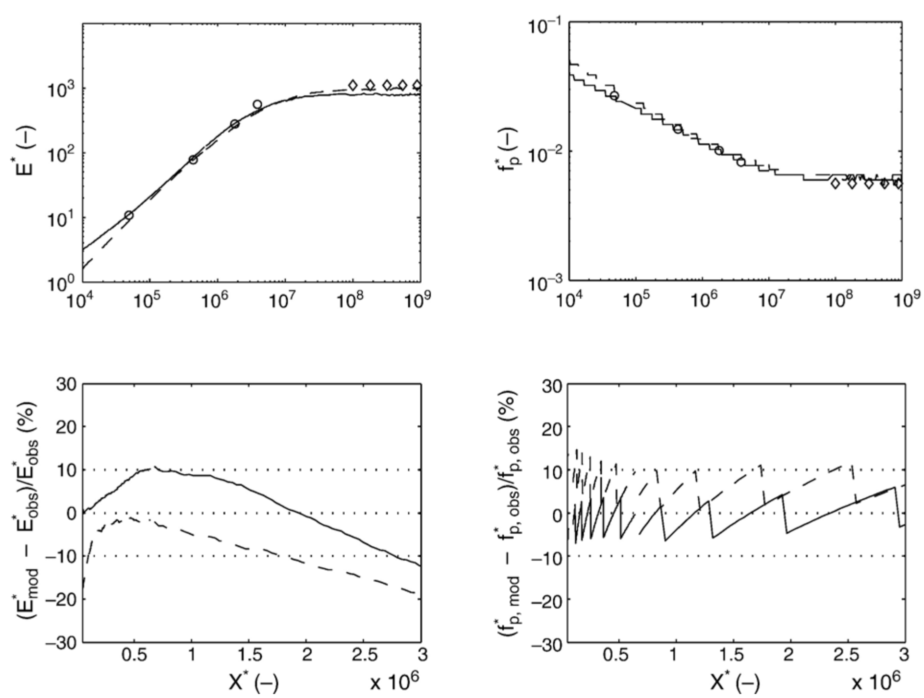

Fig. 2. Deep water, fetch-limited growth curves produced by the saturation-based model (solid lines) and the default model (dashed lines), both using the DIA quadruplet method. Top panels: comparison with fetch-limited relations of Kahma and Calkoen (1992) (circles) and Pierson and Moskowitz (1964) (diamonds). Bottom panels: bias of model results with respect to Kahma and Calkoen (1992) data. Results for $U_{10} = 10$ m/s.

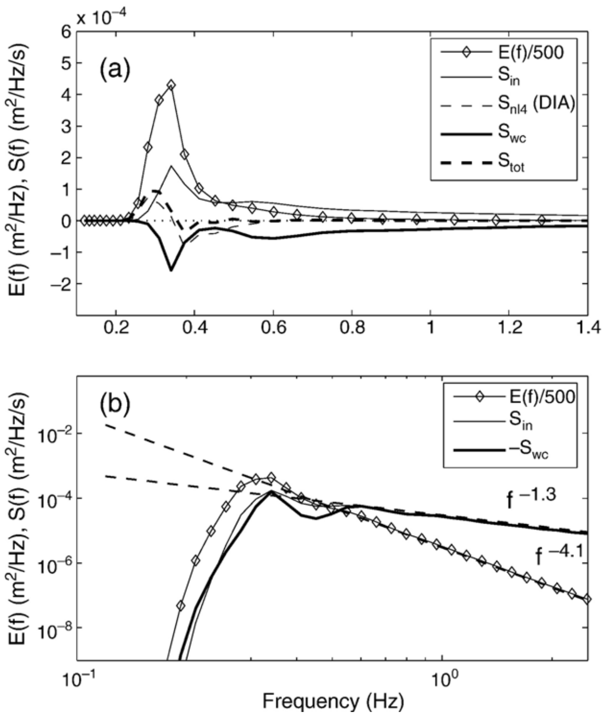

Fig. 3. Source terms produced by the saturation-based model using the DIA quadruplet method. Panel (a): variance spectrum and all source terms on a linear scale, panel (b): variance spectrum and source terms of wind input and dissipation (absolute value) on logarithmic axes, with power law fits (dashed lines). Result for deep water, fetch-limited growth simulations with $U_{10}=10$ m/s, at a fetch of $X^*=7\times10^5$.

energy and peak frequencies adequately over a wide range, (b) are in general agreement with the observations of Kahma and Calkoen (1992) (composite dataset) and (c) reach an equilibrium level at the Pierson and Moskowitz (1964) fetch range. The bottom panels of Fig. 2 present the biases of the two models' results with respect to the growth curves of Kahma and Calkoen—the fetch range typically of interest to coastal wind–wave modelling. The calibrated saturation-based model produces smaller biases in both dimensionless energy and peak frequency than the default model. In particular, the mean overprediction of the peak frequency by the default model is corrected. (The saw-tooth shape of the bias curves of peak frequency is due to the discrete nature of the frequency domain in the model; it is the mean of these oscillations that is compared with the observations.) At very large fetches, the saturation-based model underpredicts the equilibrium level of dimensionless energy of Pierson and Moskowitz (1964) (top left-hand panel of Fig. 2). It will be demonstrated in Section 3.3 that this underprediction can be corrected by combining the saturation-based model with a more accurate expression for quadruplet interactions.

Fig. 3 presents the spectral shapes of the computed source functions as well as their sum, as converged, at a dimensionless fetch of $X^*=7\times10^5$. Fig. 3(b) shows that in the spectral range above 1.5 times the peak frequency, the variance spectrum has an $f^{-4.1}$ decay, which is close to the desired tail shape found in observations. In this region the dissipation function reduces as $f^{-1.3}$, similar to the wind input function. This reflects the transition from an f^{-1} to an f^{-2} frequency scaling of these two terms at this intermediate wave age (u_*/c at the spectral peak is 0.08). At frequencies just below the spectral peak, the whitecapping term is weaker than the wind input term (Fig. 3 (a) and (b)). This is in contrast to the Komen et al. (1984) wind and whitecapping combination, where these terms are roughly of the same magnitude (result not shown). The dissipation below the spectral peak is relatively low because the saturation

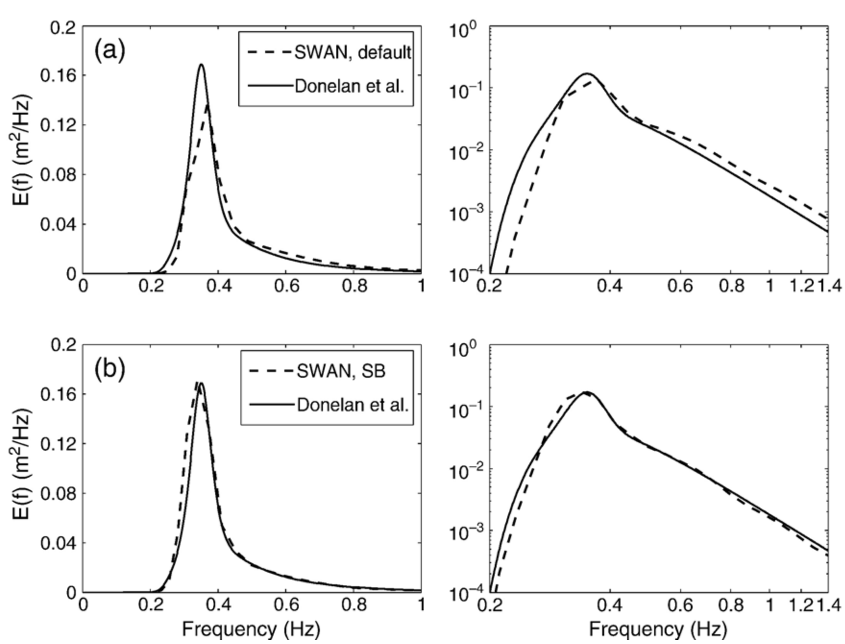

Fig. 4. Deep water fetch-limited spectra produced using the default model (row (a)) and the saturation-based model (SB) (row (b)). Spectra on the left are repeated on the right on logarithmic axes. Results for $U_{10}=10$ m/s at $X^*=6\times10^5$.

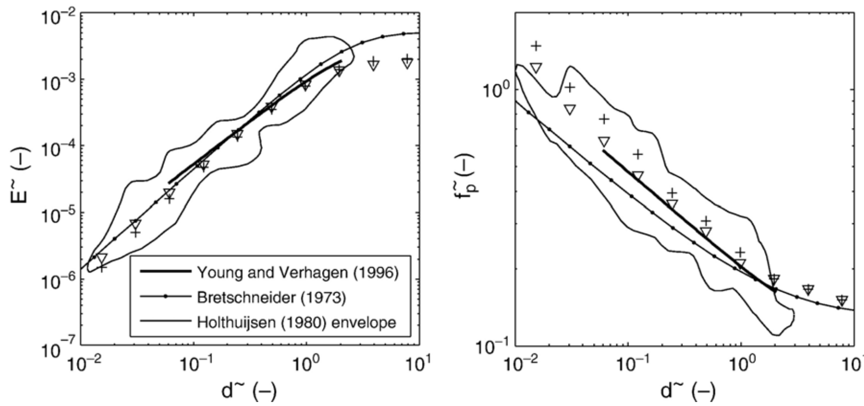

Fig. 5. Depth-limited growth curves produced by the saturation-based model (inverted triangles) and the default model (plusses). Observations as indicated. Results for U_{10} = 10 m/s.

spectrum $B(k)$ has low values in this spectral region. This represents a situation in which waves cease to dissipate energy through breaking.

Fig. 4 compares the spectra produced by the default and saturation-based models respectively with the parametric spectral shape of Donelan et al. (1985), parameterised with the peak

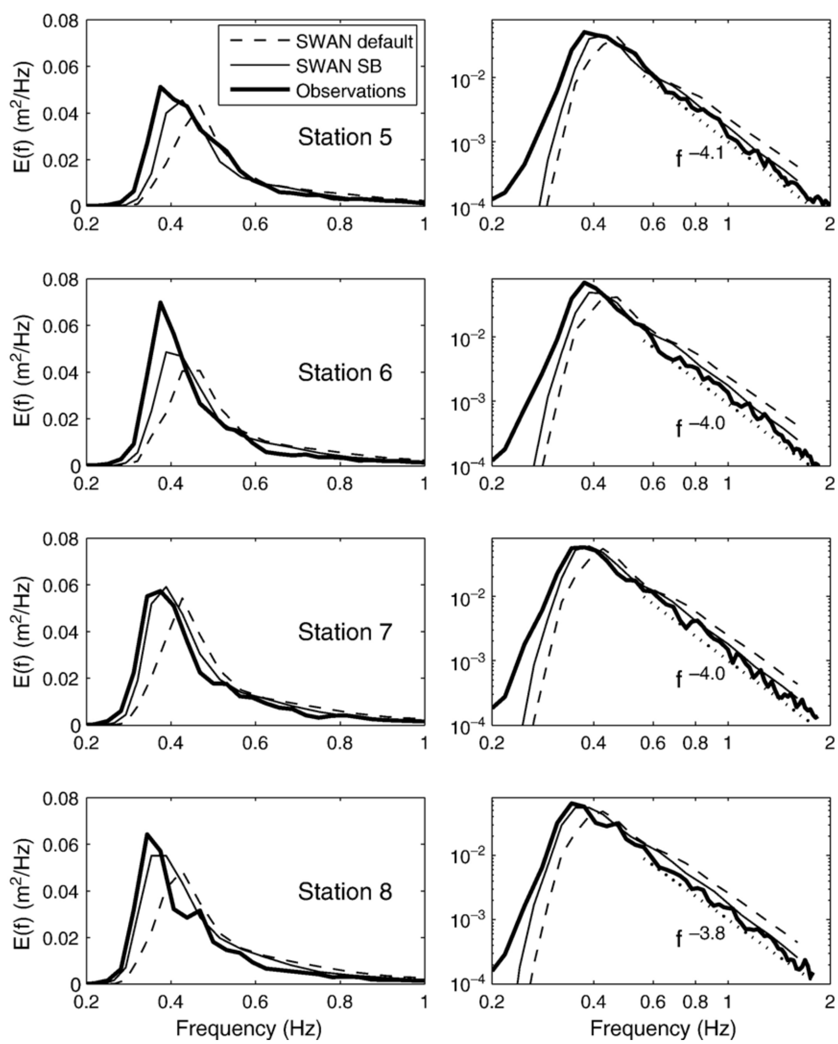

Fig. 6. Simulations of depth-limited wave growth in Lake George, Australia. Spectra produced by the saturation-based model and by the default model, both using the DIA. Spectra on the left are repeated on the right on logarithmic axes. Observations are of Young and Verhagen (1996), with the dotted lines indicating the power law slopes of the observed spectral tails. Average wind speed is 10.8 m/s.

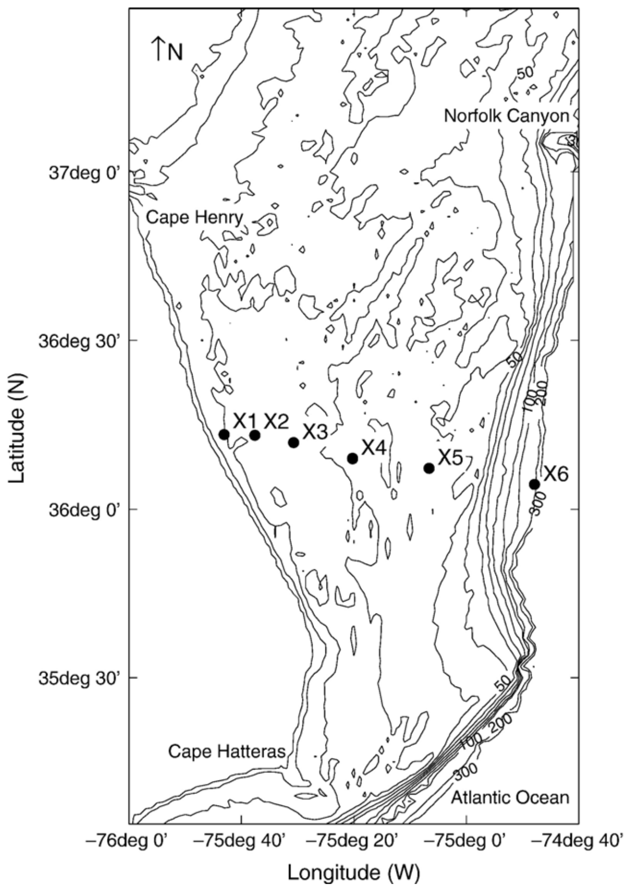

Fig. 7. Bathymetry of the North Carolina shelf during SHOWEX (1999), including the locations of the observation stations X1 to X6 (after Ardhuin et al., in press).

frequency and total energy of Kahma and Calkoen (1992). The results shown are for a dimensionless fetch of $X^* = 6 \times 10^5$, which lies within the Kahma and Calkoen fetch range. As above, the

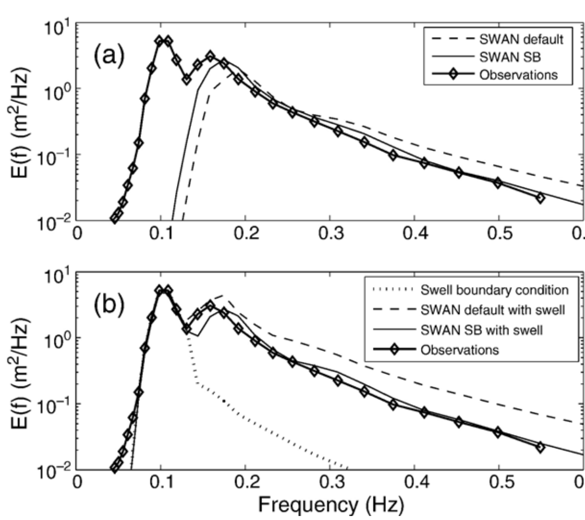

Fig. 8. Results of simulations over the North Carolina shelf at downwind Station X6. (a) Spectra of the saturation-based and default models in simulations without swell. (b) Corresponding results of simulations with ambient swell. Average wind speed is U_{10}=9.5 m/s.

default model produces some overestimation of the peak frequency, and in the energy-containing tail region ($1.5 < f/f_p < 3$) predicted energy levels are higher than those of the Donelan et al. spectrum. By contrast, the saturation-based model produces a lower peak frequency, which slightly underpredicts the observed value, and a tail that is lower in energy than with the default model, improving agreement with the Donelan et al. spectrum. As noted above, this is due to the distribution of the saturation spectrum $B(k)$, which results in greater dissipation in the spectral tail, and less around the peak than with the Komen et al. (1984) expression. The results produced by the saturation-based and default models also differ in their respective directional distributions. These are discussed in Section 3.3 below.

3.1.2. Depth-limited growth

The preceding section presented the calibration of the saturation-based model for deep water. Subsequently, the calibration of the saturation-based model for finite depth situations, using observations of idealised depth-limited growth, is outlined. Fig. 5 compares the depth-limited growth results of the saturation-based model (10) and (12) with those of the default model. Here $\tilde{E} = g^2 E_{tot} / U_{10}^4$ and $\tilde{f}_p = f_p U_{10}/g$ are the dimensionless energy and peak frequency respectively and $d = gd/U_{10}^2$ the dimensionless depth. The parameters of (12) retained their values as set in the deep water calibration. For both models, the shallow water source terms have been applied with their default formulations and parameter values (Booij et al., 1999), namely: bottom friction according to Hasselmann

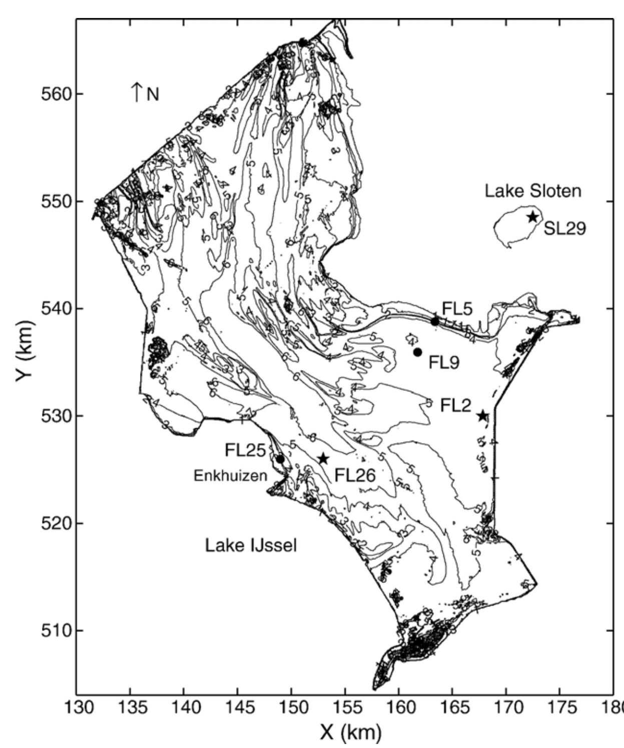

Fig. 9. Map of Lake IJssel, The Netherlands, including the locations of wave (dots) and combined wave and wind (stars) observation stations. Depth contours in m below NAP. The outline of Lake Sloten is shown to the same scale for comparison (after Bottema, 2004).

Table 1
Details of selected Lake IJssel cases

Case	Y-A	Y-B	Y-C	Y-D
Date	2/10/1999	27/10/2002	12/11/2002	2/4/2003
Time	3–4 h	14 h20–15 h20	13–14 h	14–15 h
Water level (m NAP)	−0.12	+0.23	−0.25	−0.11
Wind speed (m/s)	15.2	23.8	10.3	15.1
Wind dir. (deg. N)	215°	249°	192°	325°

et al. (1973) with friction coefficient $C_{JON}=0.067$ m^{2}s^{-3}, nonlinear triad interactions according to Eldeberky (1996), with coefficient $\alpha_{EB}=0.1$, and depth-induced breaking using Battjes and Janssen (1978), with coefficient $\alpha_{BJ}=1.0$ and breaker parameter $\gamma=0.73$. The model results are compared to the observations by Bretschneider (1973), Holthuijsen (1980) and Young and Verhagen (1996). Fig. 5 shows that the saturation-based model yields increased dimensionless energy and decreased peak frequencies compared to the default model, and that these results agree better with the observations than those of the default model. The improvement is the greatest at small dimensionless depths. To put this result into perspective, these changes in dimensionless energy and peak frequency are larger than those obtained when running the default model with either depth-induced breaking deactivated, or with the bottom friction coefficient C_{JON} reduced by half (results not shown).

To demonstrate the spectra produced by the saturation-based model in intermediate water depth, Fig. 6 presents simulation results for a field case at Lake George, Australia, from the Young and Verhagen (1996) dataset. During this measurement campaign, spectra were measured along an array of eight stations, the endmost of which (Station 8) having a fetch of 16 km. The case presented, recorded on 03/10/1993 at 17 h00 local time, has a spatially averaged wind speed of 10.8 m/s and an average water depth of about 2 m. As a result, at Station 8 the spectral peak had a dimensionless depth of $kd=1.2$, or, in relation to Fig. 5, $\tilde{d}=0.17$. Considering the relatively short fetch, stationary simulation was applied. A geographic discretisation of $\Delta x=\Delta y=200$ m and spectral discretisations of $\Delta\sigma/\sigma=0.1$ and $\Delta\theta=10°$ were used. Fig. 6 shows that the saturation-based model, as calibrated, consistently yields more accurate predictions of the spectral peak frequency and energy than the default model. Furthermore, energy levels in the spectral tail are consistently lower than in the default model, improving the agreement with observations. On the basis of the results presented in Figs. 5 and 6, it can be concluded that the saturation-based model can be applied over finite water depths without alteration to the default shallow water source terms.

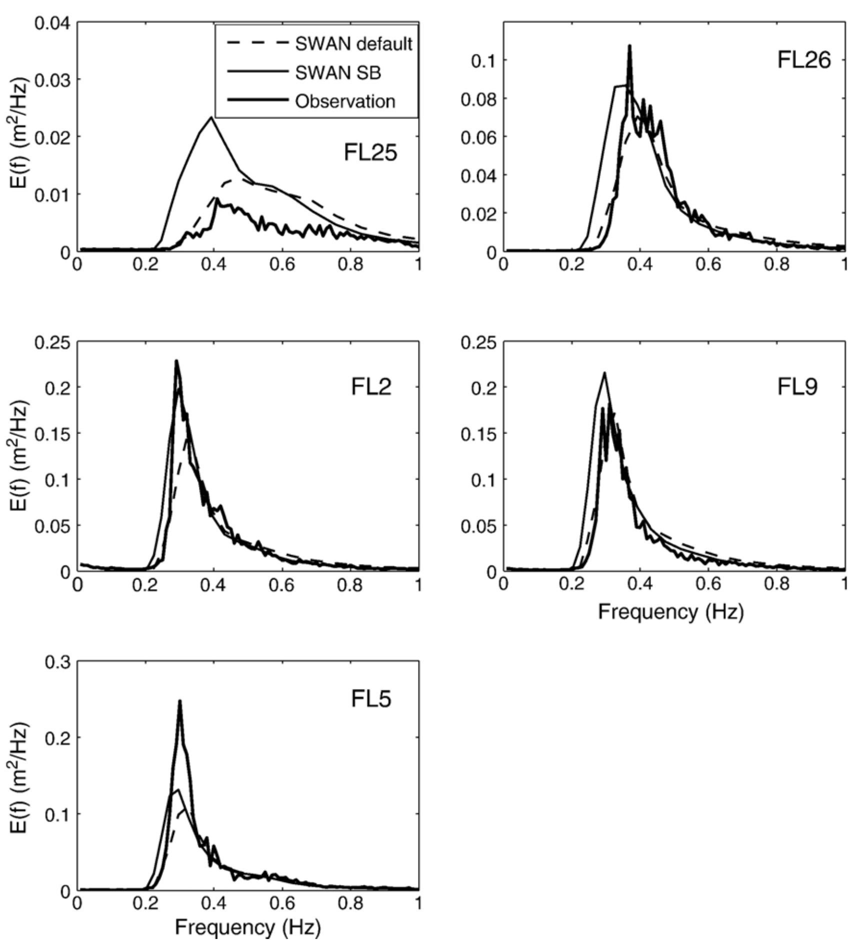

Fig. 10. Simulated spectra at five observation points in Lake IJssel for case Y-C. Wind speed $U_{10}=10.3$ m/s and direction 192° (SSW). Compared are the simulation results of the saturation-based and default models, and observations.

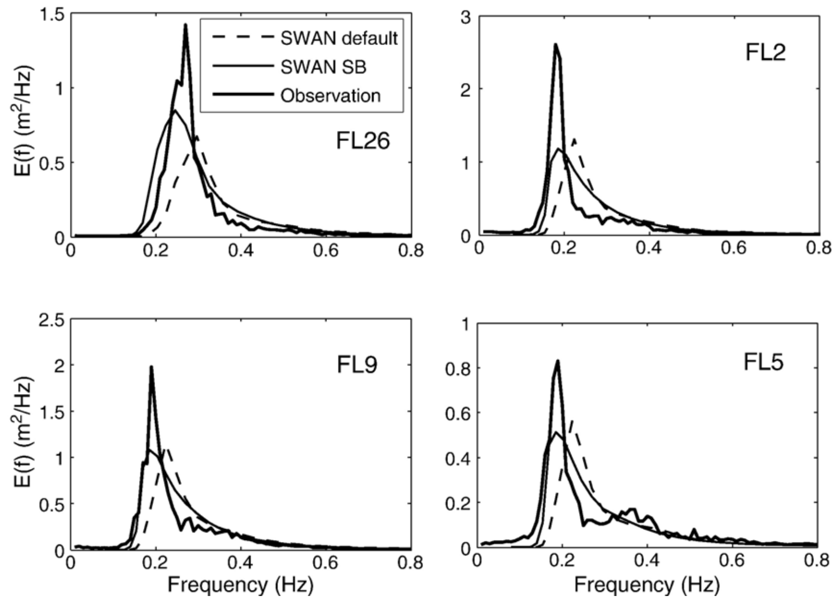

Fig. 11. Simulated spectra at four observation points in Lake IJssel for case Y-B. Wind speed U_{10}=23.8 m/s and direction 249° (WSW). Compared are the simulation results of the saturation-based and default models, and observations.

3.2. Evaluation

In this section the saturation-based model (10) and (12), as calibrated for use with the DIA, is evaluated on the basis of a number of field cases. These include a shelf sea case with combined swell-sea conditions and a number of cases recorded at two shallow lakes.

3.2.1. Shelf sea with combined swell and wind-sea

A primary aim of this study is to address the spurious behaviour of the default SWAN model under combined swell-sea conditions, which occurs due to the dependence of the Komen et al. (1984) whitecapping expression on mean spectral quantities. This section compares the performance of the default and saturation-based model versions, both using the DIA, under such conditions. Ardhuin et al. (in press) present results of field measurements off the coast of North Carolina, USA, in which deep water wave growth under near-idealised conditions was observed in combination with oceanic swell. Fig. 7 shows the shelf sea area over which this mixed wave field was observed, including the array of wave observation stations X1 to X6. On 03/11/1999, from 12 h00 to 17 h00 local time, a fairly steady and uniform wind of about U_{10}=9.5 m/s blew offshore from the west, at an angle of 20°–30° to shore normal. During this time, a moderate swell from ESE prevailed, nearly opposing the wind. Ardhuin et al. show that whereas the observed wind-sea growth at Stations X1 to X6 did not appear to be affected by the presence of the opposing swell, numerical models using the whitecapping expressions of Komen et al. (1984) significantly overestimate the wind-sea for this field case where swell is present. The simulations conducted by Ardhuin et al. are repeated here using the default and saturation-based SWAN models.

Non-stationary simulations, running from 02/11/1999 23 h00 to 03/11/1999 23 h00, were performed over the area 76°–74°40′ W, 34°30′–38° N with a spatial resolution of 1/60° and a time step of 600 s. A frequency resolution of $\Delta\sigma/\sigma=0.1$

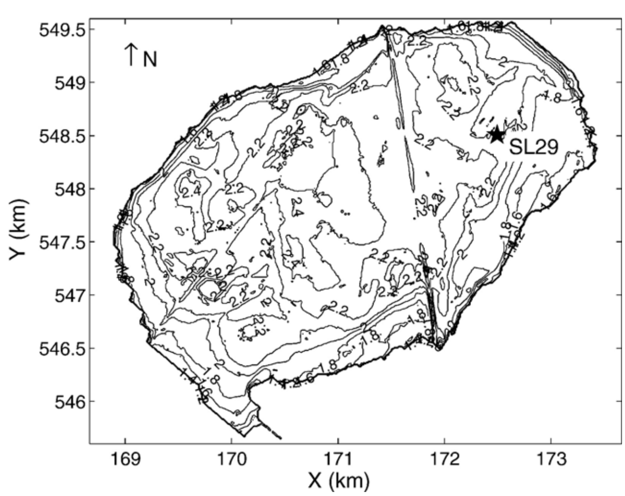

Fig. 12. Map of Lake Sloten, The Netherlands, including the location of the wave and wind observation station SL29. Depth contours in m below NAP (after Bottema, 2004).

Table 2
Details of selected Lake Sloten cases

Case	SL-A	SL-B	SL-C	SL-D	SL-E
Date	27/10/2002	26/2/2002	12/2/2002	10/2/2002	10/10/2002
Time	15–16 h	14–15 h	13–14 h	4–5 h	12–13 h
Water level (m NAP)	−0.45	−0.29	−0.43	−0.47	−0.47
Wind speed (m/s)	21.4	20.8	15.0	11.0	10.6
Wind dir. (deg. N)	252°	243°	253°	245°	88°

and a directional resolution of $\Delta\theta = 10°$ were used. A non-stationary wind field was applied, which was interpolated from observations taken at a number of offshore and nearshore stations in the area. Two sets of simulations were conducted, one without swell and one with swell included. In the latter series of simulations, the swell energy measured at the offshore Station X6 was applied as boundary condition at the offshore boundary running along 74°40′ W.

Fig. 8(a) presents the results of the first set of simulations, namely those in absence of swell, at the downwind Station X6. Following Ardhuin et al., the results were averaged over the period 12 h00–17 h00, to reduce scatter. Ardhuin et al. find that the wind-sea component of the observed spectra agrees well with well-known growth curves (e.g. Kahma and Calkoen, 1992), from which they conclude that the wind-sea growth was not affected by the prevailing swell. The spectrum produced by the default SWAN model supports this view: the spectrum computed in the absence of swell agrees fairly well with the wind-sea part of the observed spectrum, taking into account the overestimation of the peak frequency and of energy in the spectral tail with the default model, discussed in the sections above (for pure wind-sea growth). The wind-sea-only simulation with the saturation-based model also yields fair agreement with the wind-sea part of the observed spectrum, with its peak frequency, peak energy density and spectral tail agreeing better with observations than those of the default model.

Fig. 8(b) presents the corresponding model results for simulations in which the prevailing swell was included at the eastern model boundary, so that the wind-sea developed in the presence of a swell field with a peak period of about 10 s. The default SWAN model is significantly influenced by the swell, as found by Ardhuin et al. Energy levels at both the spectral peak and tail are increased by about a factor 2. The peak frequency is also reduced, which partly corrects its overprediction in simulations with wind only. However, as discussed in the introduction, this improvement is spurious: swell reduces the mean spectral steepness, reducing the amount of whitecapping dissipation, which leads to excessive wind–wave growth. By contrast, the saturation-based model, in which the whitecapping dissipation does not depend on mean spectral quantities, is unaffected by the presence of the swell, and yields the same fair agreement with the observations as in the wind only case.

3.2.2. Shallow lakes

To evaluate the saturation-based model's performance in finite depth water, this section considers the simulation of a collection of field cases recorded at Lake IJssel and Lake Sloten, two shallow lakes in The Netherlands. Fig. 9 presents a contour

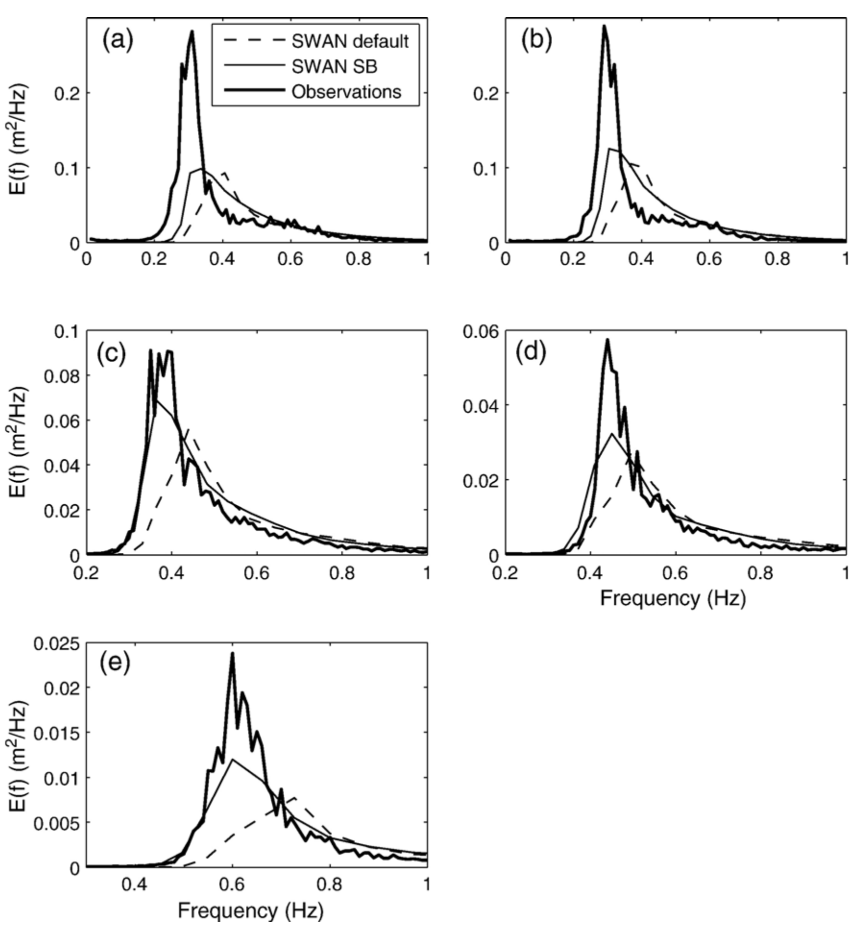

Fig. 13. Simulated spectra of five cases observed at Lake Sloten: (a) SL-A, with wind speed $U_{10} = 21.4$ m/s, WSW, (b) SL-B, $U_{10} = 20.8$ m/s, WSW, (c) SL-C, $U_{10} = 15.0$ m/s, WSW, (d) SL-D, $U_{10} = 11.0$ m/s, WSW and (e) SL-E, $U_{10} = 10.6$ m/s, E. Compared are the simulation results of the saturation-based and default models, and observations.

plot of Lake IJssel, including the locations of five wave observation stations. Winds were measured at Stations FL2 and FL26. Lake IJssel is relatively shallow, with a depth of about 5 m at Station FL26 in the west, sloping to a depth of about 4 m at Stations FL2 and FL9 towards the east. Bottema (2004) selected four cases suitable for model evaluation from measurements at Lake IJssel, based on the following criteria: (a) the measured wind field was to be spatially uniform (differing by less than 5% at Stations FL2 and FL26) and (b) stationary conditions were to prevail for at least 2 h. These four cases, labelled Y-A to Y-D, are listed in Table 1. Water levels are given relative to the Dutch datum NAP, and the direction from which the wind is blowing is measured clockwise from the North. On the basis of wind speed, these storm events can be considered to range from deep water situations (case Y-C) to intermediate water depth situations (case Y-B). Considering the small geographical extent of the model area and the stationarity of the physical conditions, model runs were conducted in

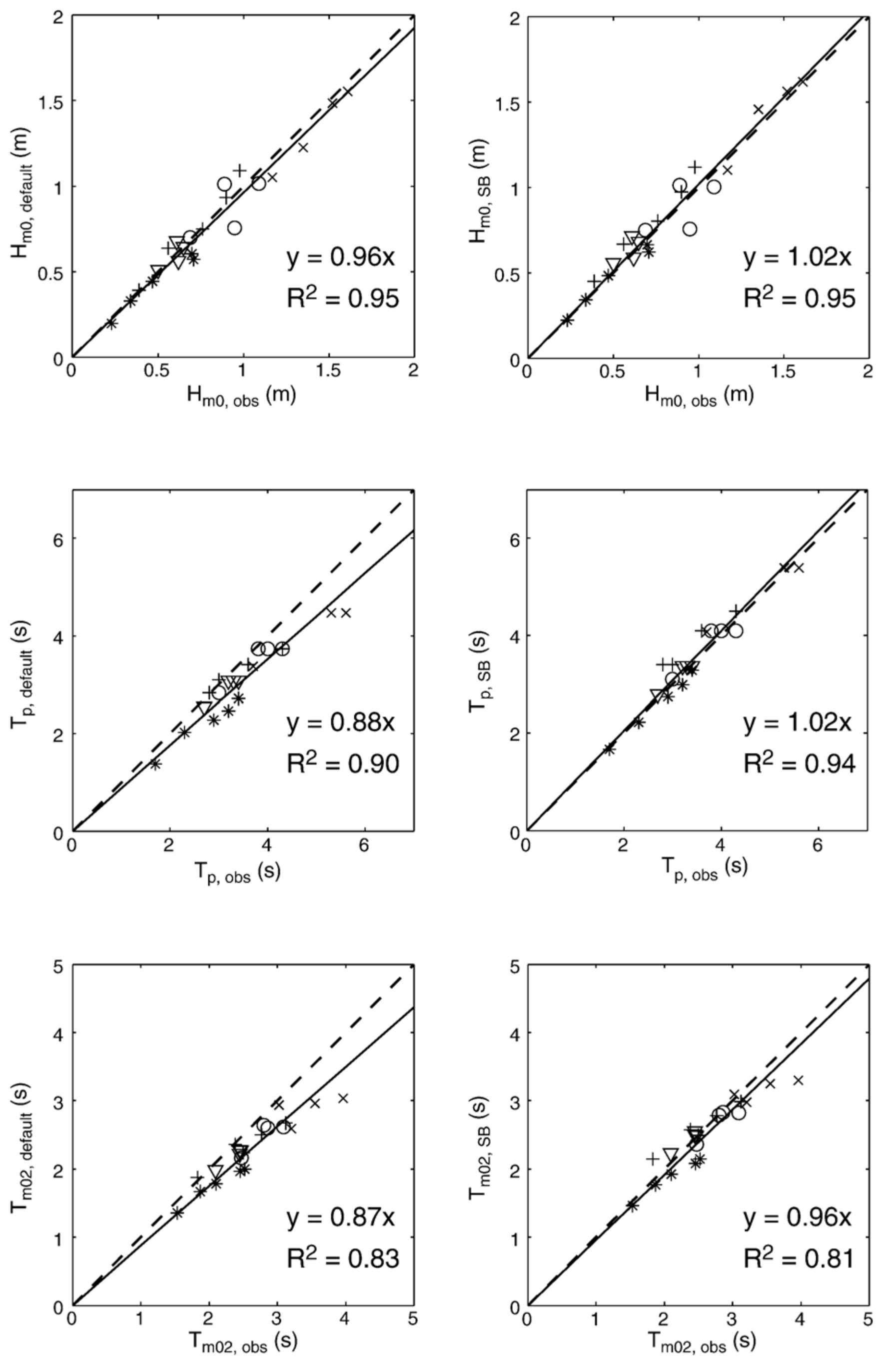

Fig. 14. Scatter plots of H_{m0}, T_p and T_{m02} produced by the default (left-hand panels) and saturation-based (right-hand panels) models versus observations, for the Lake IJssel and Lake Sloten simulations. Included are the following cases from Tables 1 and 2: Y-A (○), Y-B (×), Y-C (▽), Y-D (+) and SL-A to SL-E (∗). Lines of perfect correlation (dashed) and best fit (forced through the origin, solid), including its formula and R^2 correlation coefficient, are also shown.

stationary mode. Wind fields were applied spatially uniform. A spatial discretisation of $\Delta x = \Delta y = 250$ m and spectral discretisations of $\Delta\sigma/\sigma = 0.1$ and $\Delta\theta = 10°$ were used.

Figs. 10 and 11 present the simulation results for two of the selected Lake IJssel cases. Fig. 10 shows that for case Y-C (moderate wind speed) the peak frequencies produced by the default model agree well with the observations at Stations FL9 and FL26, but are slightly higher than the observations at the downwind locations FL2 (deep) and FL5 (shallow). Similarly, total energy is fairly well predicted by the default model at Stations FL9 and FL26, but underpredicted at the downwind stations FL2 and FL5. By contrast, the saturation-based model predicts the peak frequencies well at some stations and underpredicts them somewhat at others. The values of total energy produced by the saturation-based model are consistently higher than those of the default model, improving on the latter's underestimations at downwind stations FL2 and FL5. The exception to these results is the upwind location FL25, which has a short fetch of about 1 km ($X^* \approx 7 \times 10^4$ for this wind speed). At this station, energy levels are strongly overpredicted by both the default and the saturation-based models, even though, for a corresponding dimensionless fetch X^*, the saturation-based model's result agrees with the Kahma and Calkoen (1992) growth curve (see Fig. 2). Sensitivity analyses suggest that these overpredictions may be due to the use of a spatially uniform wind field, which does not take into account a local decrease in wind speed offshore of the land–sea transition, as described for example by Taylor and Lee (1984). Other possible explanations, pointed out by one of our reviewers, are that the conventional wind input expressions applied in the model may overestimate the momentum transfer to this very young wave field (Donelan et al., 2006) or that at these early stages of development the waves themselves behave in a non-self-similar fashion, falling outside the current wind–wave modelling paradigm (Badulin et al., 2005). Consequently, the verifiability of model results at this station remains uncertain, and the results at this station are omitted from the remainder of the evaluation.

Fig. 11 presents the results of case Y-B, where the wind came from the same directional quadrant as in case Y-C, but had a much higher speed. Under these conditions, the default model consistently overpredicts the peak frequency and underpredicts the total wave energy. This frequency overprediction is most evident at the downwind locations FL2, FL9 and FL5. By contrast, the saturation-based model accurately predicts the peak frequency at most locations, and the predicted total energy is slightly higher than with the default model. The remaining cases Y-A and Y-D, of which the spectra are not shown, yield similar results to those discussed.

Lake Sloten is considerably smaller and shallower than Lake IJssel, with a greatest length of 4 km and depths of about 1.6 to 1.8 m in the cases considered here (its outline is included in Fig. 9 for comparison). Fig. 12 presents a contour plot of Lake Sloten, indicating its only wave and wind observation station, SL29. Bottema (2004) selected five cases for this site, cases SL-A to SL-E given in Table 2, based on the criteria that (a) stationary conditions prevailed, and (b) that the resulting wave fields in these cases were representative of the mean of all observations taken. Of these, cases SL-A to SL-D feature moderate to strong WSW winds with a fetch of 3 km, and case SL-E a moderate easterly wind, with a short fetch of 1 km. The wave fields in the high wind speed cases have dimensionless

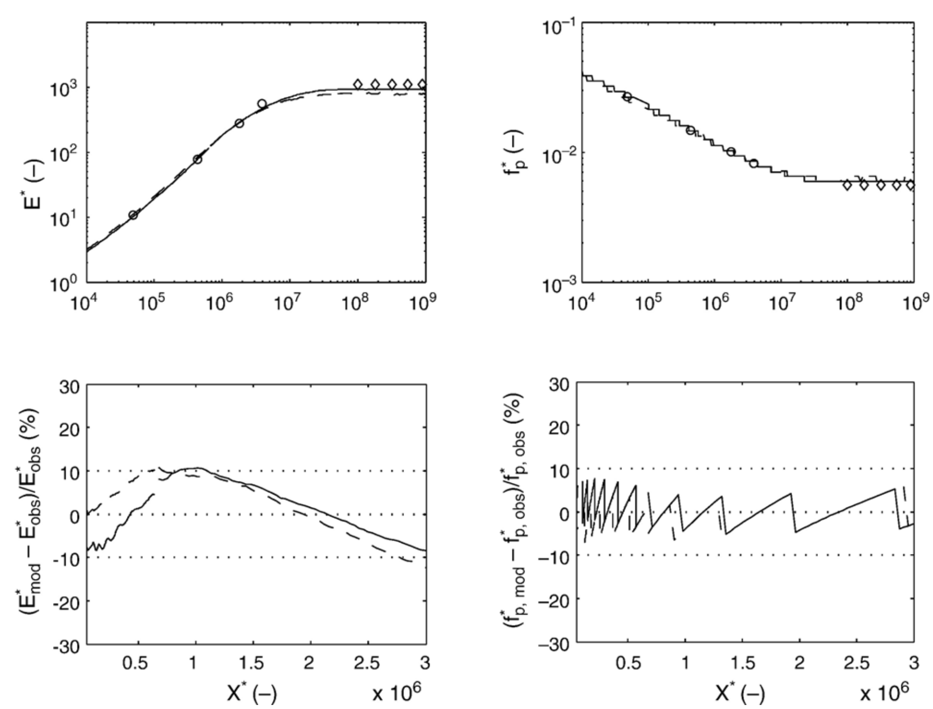

Fig. 15. As in Fig. 2, but with the growth curves produced by the saturation-based model combined with the WRT method (solid lines) compared with those by the saturation-based model using the DIA (dashed lines). Results for $U_{10} = 10$ m/s.

depths at the spectral peak as low as $k_p d=0.9$ (or $\tilde{d}=4\times10^{-2}$). Simulations were conducted in stationary mode, using a spatial discretisation of $\Delta x=\Delta y=40$ m and spectral discretisations of $\Delta\sigma/\sigma=0.1$ and $\Delta\theta=10°$.

Fig. 13 presents the simulation results for these five cases at Station SL29. With the default model, peak frequencies are overpredicted and the energy density at the peak is underpredicted throughout. The predictions of the saturation-based model consistently improve on these results. This improvement is most significant, and the correlation with observations the best, for the cases SL-C, SL-D and SL-E, where moderate to moderately high wind speeds prevailed. In cases SL-A and SL-B, where wind speeds were high, peak frequencies are still somewhat overestimated and energy levels at the spectral peak remain significantly underpredicted by the saturation-based model. Furthermore, particularly for these two cases, the observed spectral shape has a large peak enhancement, that is not found in the simulation results of either the saturation-based or the default models.

Fig. 14 presents a comparative summary of the performance of the saturation-based model for the Lake IJssel and Sloten simulations in the form of scatter plots of significant wave height, and peak and mean periods. The left-hand panels of Fig. 14 present the performance of the default model: significant wave heights are well predicted, with an average bias of 4%, but peak and mean periods are underpredicted, with average biases −12% and −13% respectively. By contrast, the saturation-based model (right-hand panels of Fig. 14) yields a small overestimation of significant wave height, with an average bias of +2%, and a similar, high correlation coefficient. The greatest improvement in performance due to the saturation-based model is found in the period measures: the peak period, underpredicted by the default model, is overpredicted by a mere +2% and has a higher correlation coefficient; the underprediction of the mean period T_{m02} is reduced to −4%, albeit with a slightly lower correlation coefficient.

3.3. Saturation-based model with exact quadruplet interactions

The simulations presented in this paper thus far were done by combining the saturation-based model with the DIA method for calculating quadruplet interactions. Because of its computational efficiency, the DIA is currently used in most operational wave models. However, the DIA computes only a small number of the complete set of quadruplet interactions, and therefore yields a fairly inaccurate representation of this process (Van Vledder and Bottema, 2003). In this section we shall highlight some characteristics of the saturation-based

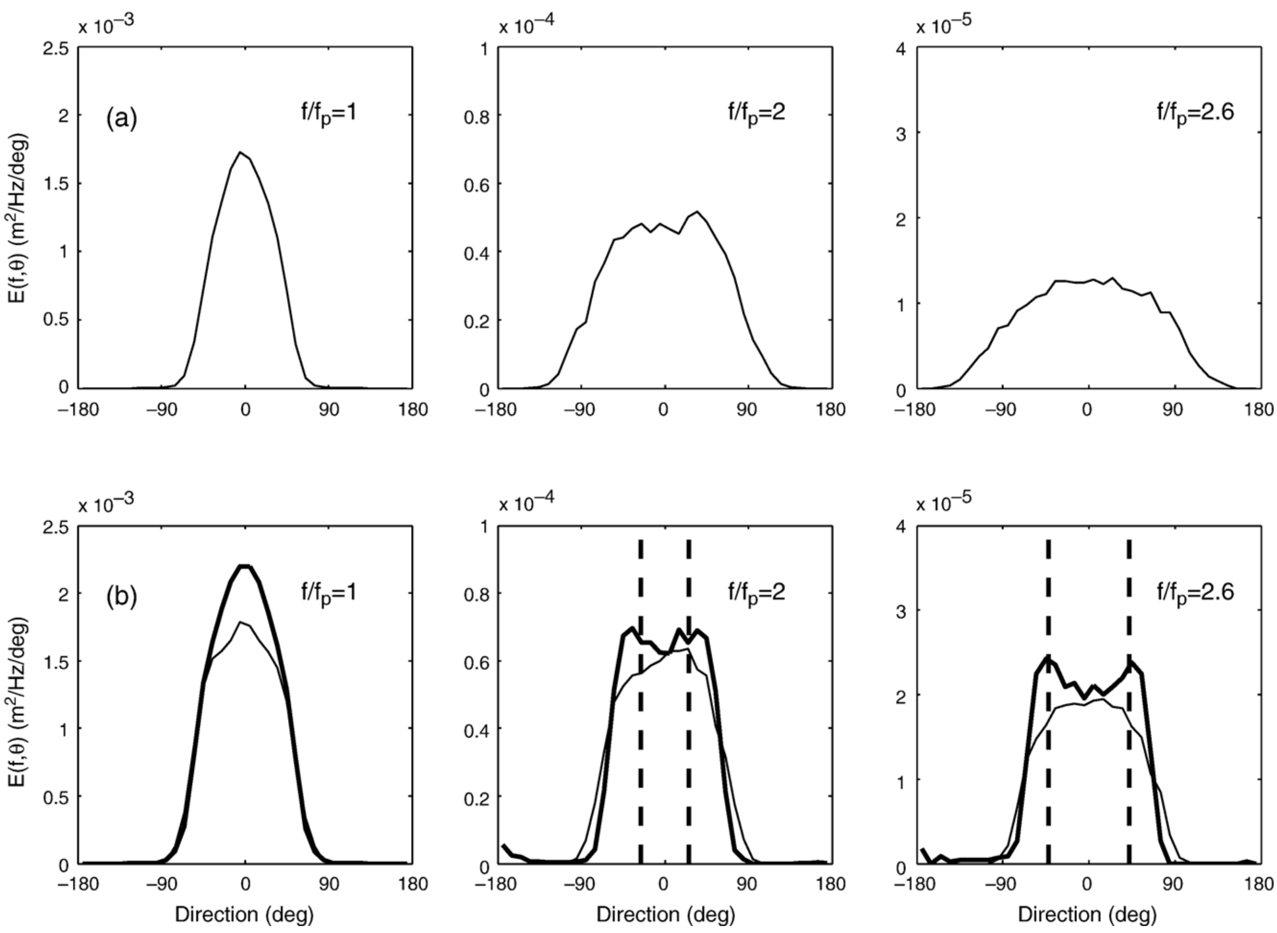

Fig. 16. Directional distributions at the spectral peak and within the energy-containing tail produced using respectively the default model (row (a)) and the saturation-based model (row (b)). Results for deep water, fetch-limited growth with $U_{10}=10$ m/s at $X^*=6\times10^5$. Thin solid lines are results produced using the DIA and thick lines those using the WRT method. Dashed lines indicate the location of the bi-modal peaks observed by Hwang et al. (2000).

model (10) and (12) when combined with a complete (exact) description of quadruplet interactions. For this, the WRT method, as reprogrammed by Van Vledder (2005), was used.

Fig. 15 presents a comparison of the deep water fetch-limited growth curves produced by the saturation-based model combined with the WRT and DIA quadruplet expressions respectively. Due to the replacement of the DIA by the WRT method in (1), it was required to recalibrate the parameters of (12) to $C_{\mathrm{ds}}=5.0\times10^{-5}$ and $B_{\mathrm{r}}=1.95\times10^{-3}$. Similar to the growth curves produced by the saturation-based model using the DIA, the combination using the WRT method yields good fits to the growth curves of dimensionless energy and peak frequency in the Kahma and Calkoen (1992) fetch range. However, when combined with the WRT, the saturation-based model yields a better estimate of the Pierson and Moskowitz (1964) equilibrium level than when combined with the DIA. The difference is due to the somewhat different evolution of the spectral peak frequency in the two models (resulting from the differences in the quadruplet expressions), and also the somewhat weaker whitecapping dissipation in the model using the WRT.

Characteristic differences between the results of the saturation-based model, using the WRT and DIA respectively, and those of the default model, are also found in their respective directional distributions. Fig. 16 shows that at frequencies higher than the peak, the saturation-based model, using the DIA, produces narrower directional distributions than the default model. A similar finding was reported by Alves and Banner (2003) using (5). They ascribed it to the greater strength of the saturation-based whitecapping expression relative to the quadruplet term in this spectral region. This decreases the energy levels at angles away from the mean propagation direction. In addition, a characteristic consequence of using an exact quadruplet method is that the directional distribution becomes bi-modal at higher frequencies, as observed in the field by, for example, Hwang et al. (2000). Fig. 16 shows that the bi-modal directional distribution produced by the saturation-based model using the WRT agrees well with their observations. This bi-modality is also found with other spectral models when using exact quadruplet interactions (e.g. Banner and Young, 1994).

From the above it is seen that the results of the saturation-based model improve somewhat when combined with the WRT method. However the benefits obtained by using the more detailed description of quadruplet interactions are offset by longer computational times—simulations using the WRT method require 300 times as much computational time as those using the DIA. It is concluded that for typical coastal engineering applications the improvement in model results obtained by combining the saturation-based model with the WRT does not justify this large increase in computational cost.

4. Discussion and conclusions

This study investigated whether the accuracy of SWAN, specifically with regard to period measures, could be improved by implementing a whitecapping expression based on that of Alves and Banner (2003) in combination with a wind input term based on that of Yan (1987). The resulting source term combination was calibrated against fetch- and depth-limited growth curves and subsequently evaluated for a shelf-sea field case with combined swell-sea wave conditions and a number of shallow water field cases. In addition, the effect of combining these source terms with a complete description of quadruplet interactions, as opposed to the DIA approximation, was investigated. The following conclusions can be drawn from this study:

(a) In idealised fetch-limited growth simulations, the investigated saturation-based model, using the DIA, yields more accurate estimates of dimensionless energy and peak frequency than the default model within the Kahma and Calkoen (1992) fetch range. In particular, the peak period underprediction of the default model is corrected by this new model. The investigated model also yields lower energy levels in the spectral tail than the default model, bringing it in closer agreement with observations.

(b) In idealised depth-limited growth simulations, the investigated model yields higher dimensionless energy and lower dimensionless peak frequencies than the default model values, improving agreement with observations.

(c) Under combined swell-sea conditions, the results of the investigated model, which treats dissipation as a local process in frequency space, are not affected by the presence of background swell. This is in contrast to the performance of the default model, which has been shown to greatly overpredict the wind-sea part of the spectrum under such conditions due to a dependence of its dissipation expression on mean spectral steepness. It should be noted that even though decoupling the dissipation of swell and sea appears to improve model reliability, some studies, e.g. Banner et al. (1989) and Young and Babanin (2006), have produced evidence of coupling of dissipation across the spectrum. Such effects could be parameterised and added as additional dissipation terms to the action balance equation (1), as proposed by Young and Babanin (2006), for example, rather than being included as multiplication factors, as proposed by Alves and Banner (2003).

(d) In shallow lakes, at depths at which the source terms of wind input and whitecapping dominate over purely shallow water processes, the investigated model yields satisfactory results. The investigated model yields higher peak periods and mean periods than the default model, which corrects the underprediction of these parameters by the latter for the most part. The investigated and default models generally perform equally well in predicting significant wave height, yielding small biases and high correlations. An exception to these encouraging results is found over very short dimensionless fetches, such as for station FL25 at Lake IJssel, under SW wind, where the total spectral energy is significantly overestimated. Such discrepancies may be caused by insufficient accuracy in the wind data, exclusion of some important wind input mechanisms (e.g. Donelan et al., 2006), or non-self-similar behaviour by the waves (e.g. Badulin et al., 2005). It was also found that at small dimensionless depths, such as the strong wind cases at Lake Sloten, both the spectral peak period and the peak enhancement are still underestimated by the investigated model. This may point to shortcomings in the shallow water source terms employed, or may again be due to neglected wind input mechanisms or non-self-similar behaviour in these strongly forced, shallow water waves.

(e) Combining the saturation-based model with the WRT exact quadruplet expression, instead of the rather inaccurate DIA, yields, in addition to the improvements mentioned under (a), a better estimate of the Pierson and Moskowitz (1964) equilibrium level, and improves the details of the directional distribution at higher frequencies. However, such an exact quadruplet method requires much additional computation time, making it unsuitable for operational use. Yet, Van Vledder (2005) presents various possibilities for reducing the computational cost of the WRT method without compromising its results, and parallel computing facilities are available in SWAN (Zijlema, 2005), so that such model runs could be conducted for selected cases.

(f) Based on the findings of this study, it can be concluded that the proposed source term expressions have improved the general predictive skill of the SWAN model. We would like to stress, however, that although the skill of these parameterisations has been demonstrated, this study does not amount to a validation of the individual source terms used, nor does it attempt to establish their underlying physics.

Acknowledgements

We are grateful to Vladimir Makin for providing parts of the Alves and Banner (2003) source code and to Gerbrant Van Vledder, Fabrice Ardhuin, Tom Herbers and Marcel Bottema for useful discussions and for providing us with field cases for the evaluation of our model. We also thank our reviewers for their useful comments. This study is supported by the National Institute for Coastal and Marine Management/RIKZ of the Ministry of Transport, Public Works and Water Management, The Netherlands, through the project RKZ-1124.

Appendix A. Source term scaling

Below, the scalability of the whitecapping and wind input expressions (8) and (10) is demonstrated for weakly and strongly forced waves in deep and shallow water.

A.1. Weakly forced waves

For weakly forced waves, the wind input expression is taken to be of the form (4), which has the following scaling:

$$S_{\mathrm{in,Snyder}}(\sigma,\theta)\propto\frac{u_*}{c}\sigma E(\sigma,\theta)\propto k\ E(\sigma,\theta)\ ,\ \text{using}\ c=\sigma/k. \tag{13}$$

Under weak wind forcing, the whitecapping expression (8) has been parameterised to have $p=2$, so that its proportionality becomes:

$$S_{\mathrm{wc},p=2}(\sigma,\theta)\propto[B(k)]g^{\frac{1}{2}}k^{\frac{1}{2}}E(\sigma,\theta)\propto\left[g^{-\frac{1}{2}}k^{\frac{1}{2}}\right]g^{\frac{1}{2}}k^{\frac{1}{2}}E(\sigma,\theta) = k\ E(\sigma,\theta), \tag{14}$$

so that wind input and whitecapping dissipation both scale as $kE(\sigma,\theta)$, implying equal scaling in both deep water and finite depth. In deep water, with an equilibrium tail of f^{-4}, the expressions both scale as f^{-2} (since $\sigma^2=gk$).

A.2. Strongly forced waves

For strongly forced waves, the wind input expression is taken to be of the form proposed by Plant (1982), which has the following scaling:

$$S_{\mathrm{in,Plant}}(\sigma,\theta)\propto\left(\frac{u_*}{c}\right)^2\sigma E(\sigma,\theta)\propto c^{-1}k\ E(\sigma,\theta) = g^{-\frac{1}{2}}k^{\frac{3}{2}}[\tanh(kd)]^{-\frac{1}{2}}E(\sigma,\theta) \tag{15}$$

which reduces in deep water to

$$S_{\mathrm{in,Plant}}(\sigma,\theta)|_{\mathrm{deep}}\quad\propto\quad g^{-\frac{1}{2}}k^{\frac{3}{2}}E(\sigma,\theta) \tag{16}$$

Under strong wind forcing, the whitecapping expression (8) has been parameterised to have $p=4$, so that its proportionality becomes:

$$S_{\mathrm{wc},p=4}(\sigma,\theta)\propto[B(k)]^2g^{\frac{1}{2}}k^{\frac{1}{2}}E(\sigma,\theta)\propto\left[g^{-\frac{1}{2}}k^{\frac{1}{2}}\right]^2g^{\frac{1}{2}}k^{\frac{1}{2}}E(\sigma,\theta) = g^{-\frac{1}{2}}k^{\frac{3}{2}}E(\sigma,\theta). \tag{17}$$

which is the same as (16), obtained for the wind input term for deep water. Therefore, in deep water, with an equilibrium tail of f^{-4}, the expressions (16) and (17) both scale as f^{-1}. In finite depth, the wind input term scales as (15), which differs from (17) by a dimensionless factor of $[\tanh(kd)]^{-\frac{1}{2}}$.

References

Alves, J.H.G.M., Banner, M.L., 2003. Performance of a saturation-based dissipation-rate source term in modelling the fetch-limited evolution of wind waves. J. Phys. Oceanogr. 33, 1274–1298.

Ardhuin, F., Jenkins, A.D., 2006. On the interaction of surface waves and upper ocean turbulence. J. Phys. Oceanogr. 36, 551–557.

Ardhuin, F., Herbers, T.H.C., Van Vledder, G.Ph., Watts, K.P., Jensen, R., Graber, H.C., in press. Swell and slanting fetch effects on wind wave growth. J. Phys. Oceanogr.

Babanin, A.V., Young, I.R., Banner, M.L., 2001. Breaking probabilities for dominant surface waves on water of finite constant depth. J. Geophys. Res. 106 (C6), 11659–11676.

Badulin, S.I., Pushkarev, A.N., Resio, D., Zakharov, V.E., 2005. Self-similarity of wind-driven seas. Nonlinear Process. Geophys. 12, 891–945.

Banner, M.L., Young, I.R., 1994. Modelling spectral dissipation in the evolution of wind waves. Part I: assessment of existing model performance. J. Phys. Oceanogr. 24, 1550–1571.

Banner, M.L., Jones, I.S.F., Trinder, J.C., 1989. Wave number spectra of short gravity waves. J. Fluid Mech. 198, 321–344.

Banner, M.L., Babanin, A.V., Young, I.R., 2000. Breaking probability for dominant waves on the sea surface. J. Phys. Oceanogr. 30, 3145–3160.

Banner, M.L., Gemmrich, J.R., Farmer, D.M., 2002. Multiscale measurements of ocean wave breaking probability. J. Phys. Oceanogr. 32, 3364–3375.

Battjes, J.A., Janssen, J.P.F.M., 1978. Energy loss and set-up due to breaking of random waves. Proc. 16th Int. Conf. Coastal Eng. ASCE, pp. 569–588.

Battjes, J.A., Zitman, T.J., Holthuijsen, L.H., 1987. A reanalysis of the spectra observed in JONSWAP. J. Phys. Oceanogr. 17, 1288–1295.

Bidlot, J., Abdalla, S., Janssen, P.A.E.M., 2005. A revised formulation for ocean wave dissipation in CY25R1. Technical Report Memorandum R60.9/JB/0516. Research Department, ECMWF, Reading, U.K.

Booij, N., Ris, R.C., Holthuijsen, L.H., 1999. A third-generation wave model for coastal regions, 1. Model description and validation. J. Geophys. Res. 104 (C4), 7649–7666.

Bottema, M., 2004. Testmemo SWAN40.20a (in Dutch). Rijkswater-staat/RIZA, Werkdocument 2004.090X, 90pp.

Bottema, M., De Waal, J.P., Regeling, E.J., 2003. Some applications of the Lake IJssel/Lake Sloten wave data set. Proc. 28th Int. Conf. Coastal Eng. ASCE, pp. 413–425.

Bouws, E., Günther, H., Rosenthal, W., Vincent, C.L., 1985. Similarity of the wind wave spectrum in finite depth water. 1. Spectral form. J. Geophys. Res. 90 (C1), 975–986.

Bretschneider, C.L., 1973. Shore Protection Manual. CERC, U.S. Army Corps of Engineers, Tech. Rep., vol. 4.

Donelan, M.A., 1987. The effect of swell on the growth of wind waves. Johns Hopkins APL Tech. Dig. 8 (1), 18–23.

Donelan, M.A., 2001. A nonlinear dissipation function due to wave breaking. ECMWF Workshop on Ocean Wave Forecasting, 2–4 July, 2001, Series ECMWF Proceedings, pp. 87–94.

Donelan, M.A., Yuan, Y., 1994. Wave dissipation by surface processes. Dynamics and Modelling of Ocean Waves. Cambridge Univ. Press. 532 pp.

Donelan, M.A., Longuet-Higgins, M.S., Turner, J.S., 1972. Periodicity in whitecaps. Nature 239, 449–451.

Donelan, M.A., Hamilton, J., Hui, W.H., 1985. Directional spectra of wind-generated waves. Philos. Trans. R. Soc. Lond., A 315, 509–562.

Donelan, M.A., Babanin, A.V., Young, I.R., Banner, M.L., 2006. Wave follower measurements of the wind input spectral function. Part II. Parameterization of the wind input. J. Phys. Oceanogr. 36, 1672–1689.

Eldeberky, Y., 1996. Nonlinear transformations of wave spectra in the nearshore zone. Ph.D Thesis, Fac. of Civil Engineering, Delft University of Technology, The Netherlands, 203 pp.

Hashimoto, N., Haagsma, I.J.G., Holthuijsen, L.H., 2003. Four-wave interactions in SWAN. Proc. 28th Int. Conf. Coastal Eng. ASCE, pp. 392–404.

Hasselmann, K., 1962. On the non-linear energy transfer in a gravity-wave spectrum. Part 1. General theory. J. Fluid Mech. 12 (4), 481–500.

Hasselmann, K., 1971. On the mass and momentum transfer between short gravity waves and larger-scale motions. J. Fluid Mech. 4, 189–205.

Hasselmann, K., 1974. On the spectral dissipation of ocean waves due to whitecapping. Boundary - Layer Meteorol. 6, 107–127.

Hasselmann, D., Bösenberg, J., 1991. Field measurements of wave-induced pressure over wind–sea and swell. J. Fluid Mech. 230, 391–428.

Hasselmann, S., Hasselmann, K., 1985. Computations and parameterizations of the nonlinear energy transfer in a gravity-wave spectrum. Part 1: a new method for efficient computations of the exact nonlinear transfer integral. J. Phys. Oceanogr. 15, 1369–1377.

Hasselmann, K., Barnett, T.P., Bouws, E., Carlson, H., Cartwright, D.E., Enke, K., Ewing, J.A., Gienapp, H., Hasselmann, D.E., Kruseman, P., Meerburg, A., Müller, O., Olbers, D.J., Richter, K., Sell, W., Walden, H., 1973. Measurement of wind–wave growth and swell decay during the Joint North Sea Wave Project (JONSWAP). Dtsch. Hydrogr. Z., Suppl. 12 (A8) 95 pp.

Holthuijsen, L.H., 1980. Methods of wave prediction, parts I and II (Methoden voor golfvoorspelling, delen I en II). Technische Adviescommissie voor de Waterkeringen. The Hague, The Netherlands (in Dutch).

Holthuijsen, L.H., Booij, N., 2000. Oceanic and nearshore whitecapping effects in SWAN. Proc. 6th Int. Conf. on Wave Hindcasting and Forecasting, pp. 362–368.

Holthuijsen, L.H., Herbers, T.H.C., 1986. Statistics of breaking waves observed as whitecaps in the open ocean. J. Phys. Oceanogr. 16, 290–297.

Hsiao, S.V., Shemdin, O.H., 1983. Measurements of wind velocity and pressure with a wave follower during MARSEN. J. Geophys. Res. 88 (C14), 9841–9849.

Hurdle, D.P., 1998. Wave conditions for dike design in areas protected by breakwaters. Report A314, Alkyon Hydraulic Consultancy and Research (in Dutch).

Hurdle, D.P., Van Vledder, G.Ph., 2004. Improved spectral wave modelling of white-capping dissipation in swell sea systems. Proc. 23rd Int. Conf. on Offshore Mech. and Arctic Eng.

Hwang, P.A., Wang, D.W., 2004. An empirical investigation of source term balance of small scale surface waves. Geophys. Res. Lett. 31, L15301. doi:10.1029/2004GL020080.

Hwang, P.A., Wang, D.W., Walsh, E.J., Krabill, W.B., Shift, R.N., 2000. Airborne measurements of the wavenumber spectra of ocean surface waves. Part 2. Directional distribution. J. Phys. Oceanogr. 30, 2768–2787.

Janssen, P.A.E.M., 1991. Quasi-linear theory of wind wave generation applied to wave forecasting. J. Phys. Oceanogr. 21, 1631–1642.

Kahma, K.K., Calkoen, C.J., 1992. Reconciling discrepancies in the observed growth of wind-generated waves. J. Phys. Oceanogr. 22, 1389–1405.

Katsaros, K.B., Atakturk, S.S., 1992. Dependence of wave-breaking statistics on wind stress and wave development. In: Banner, M.L., Grimshaw, R.H.J. (Eds.), Breaking Waves. Springer, pp. 119–132.

Kitaigorodskii, S.A., Krasitskii, V.P., Zaslavskii, M.M., 1975. On Phillips' theory of equilibrium range in the spectra of wind-generated gravity waves. J. Phys. Oceanogr. 5, 410–420.

Komen, G.J., Hasselmann, S., Hasselmann, K., 1984. On the existence of a fully developed wind–sea spectrum. J. Phys. Oceanogr. 14, 1271–1285.

Komen, G.J., Cavaleri, L., Donelan, M., Hasselmann, K., Hasselmann, S., Janssen, P.A.E.M., 1994. Dynamics and Modelling of Ocean Waves. Cambridge Univ. Press. 532 pp.

Longuet-Higgins, M.S., 1969a. On wave breaking and the equilibrium spectrum of wind-generated waves. Philos. Trans. R. Soc. Lond., A 310, 151–159.

Longuet-Higgins, M.S., 1969b. A nonlinear mechanism for the generation of sea waves. Philos. Trans. R. Soc. Lond., A 311, 371–389.

Longuet-Higgins, M.S., Smith, N.D., 1983. Measurement of breaking waves by a surface jump meter. J. Geophys. Res. 14C, 9823–9831.

Melville, W.K., Matusov, P., 2002. Distribution of breaking waves at the ocean surface. Nature 417, 58–63.

Miller, H.C., Vincent, C.L., 1990. FRF Spectrum: TMA with Kitaig-orodskii's f^{-4} scaling. J. Waterw. Port Coast. Ocean Eng. 116, 57–78.

Peirson, W.L., Belcher, S.E., 2005. Growth response of waves to the wind stress. Proc. 29th Int. Conf. Coastal Eng. ASCE, pp. 667–676.

Phillips, O.M., 1985. Spectral and statistical properties of the equilibrium range in wind-generated gravity waves. J. Fluid Mech. 156, 505–531.

Phillips, O.M., Posner, F.L., Hansen, J.P., 2001. High range resolution radar measurements of the speed distribution of breaking events in wind-generated ocean waves: surface impulse and wave energy dissipation. J. Phys. Oceanogr. 31, 450–460.

Pierson, W.J., Moskowitz, L., 1964. A proposed spectral form for fully developed wind seas based on the similarity theory of S.A. Kitaigorodskii. J. Geophys. Res. 69, 5181–5190.

Plant, W.J., 1982. A relation between wind stress and wave slope. J. Geophys. Res. 87 (C4), 1961–1967.

Resio, D.T., Perrie, W., 1991. A numerical study of nonlinear energy fluxes due to wave–wave interactions, part I. Methodology and basic results. J. Fluid Mech. 223, 609–629.

Resio, D.T., Pihl, J.H., Tracy, B.A., Vincent, C.L., 2001. Nonlinear energy fluxes and the finite depth equilibrium range in wave spectra. J. Geophys. Res. 106 (C4), 6985–7000.

Resio, D.T., Long, C.E., Vincent, C.L., 2004. Equilibrium-range constant in wind-generated wave spectra. J. Geophys. Res. 109, C01018. doi:10.1029/2003JC001788.

Rogers, W.E., Hwang, P.A., Wang, D.W., 2003. Investigation of wave growth and decay in the SWAN model: three regional-scale applications. J. Phys. Oceanogr. 33, 366–389.

Snyder, R.L., Dobson, F.W., Elliot, J.A., Long, R.B., 1981. Array measurements of atmospheric pressure fluctuations above surface gravity waves. J. Fluid Mech. 102, 1–59.

Taylor, P.A., Lee, R.J., 1984. Simple guidelines for estimating wind speed variations due to small scale topographical features. Climatol. Bull. 18, 3–32.

Teixeira, M.A.C., Belcher, S.E., 2002. On the distortion of turbulence by a progressive surface wave. J. Fluid Mech. 458, 229–267.

Toba, Y., 1973. Local balance in the air–sea boundary processes. III. On the spectrum of wind waves. J. Oceanogr. Soc. Jpn. 29, 209–220.

Van der Westhuysen, A.J., Zijlema, M., Battjes, J.A., 2005. Improvement of the numerics and deep-water physics in an academic version of SWAN. Proc. 29th Int. Conf. Coastal Eng. ASCE, pp. 855–867.

Van Vledder, G.Ph., 2005. The WRT method for the computation of non-linear four-wave interactions in discrete spectral wave models. Coast. Eng. 53, 223–242.

Van Vledder, G.Ph., Bottema, M., 2003. Improved modelling of nonlinear four-wave interactions in shallow water. Proc. 28th Int. Conf. Coastal Eng. ASCE, pp. 459–471.

Wu, J., 1982. Wind-stress coefficients over sea surface from breeze to hurricane. J. Geophys. Res. 87 (C12), 9704–9706.

Yan, L., 1987. An improved wind input source term for third generation ocean wave modelling. Rep. No. 87–8, Royal Dutch Meteor. Inst. 20 pp.

Young, I.R., Babanin, A.V., 2006. Spectral distribution of energy dissipation of wind-generated waves due to dominant wave breaking. J. Phys. Oceanogr. 36, 376–394.

Young, I.R., Van Vledder, G.Ph., 1993. A review of the central role of nonlinear interactions in wind–wave evolution. Philos. Trans. R. Soc. Lond., A 342, 505–524.

Young, I.R., Verhagen, L.A., 1996. The growth of fetch limited waves in water of finite depth. Part 2. Spectral evolution. Coast. Eng. 29, 79–99.

Zakharov, V.E., 1999. Statistical theory of gravity and capillary waves on the surface of a finite-depth fluid. Eur. J. Mech. B, Fluids 18, 327–344.

Zijlema, M., 2005. Parallelization of a nearshore wind wave model for distributed memory architectures. In: Winter, G., Ecer, A., Periaux, J., Satofuka, N., Fox, P. (Eds.), Parallel Computational Fluid Dynamics—Multidisciplinary Applications. Elsevier, pp. 207–214.